A First-in-Class β-Glucuronidase Responsive Conjugate for Selective Dual Targeted and Photodynamic Therapy of Bladder Cancer

Vasilii F. Otvagin[a], Lubov V. Krylova[a], Nina N. Peskova[a], Natalia S. Kuzmina[a], Ekaterina A. Fedotova[a], Alexander V. Nyuchev[a], Yuliya V. Romanenko[b], Oscar I. Koifman[b], Sergey Z. Vatsadze[c], Hans-Günther Schmalz[d], Irina V. Balalaeva[a*], Alexey Yu. Fedorov[a*]*

[a]Lobachevsky State University of Nizhny Novgorod, Gagarina av. 23, Nizhny Novgorod 603950, Russian Federation, Fax: +7 831-462-32-32

[b]Research Institute of Macroheterocycles, Ivanovo State University of Chemical Technology, 153000 Ivanovo, Russian Federation

[c]N. D. Zelinsky Institute of Organic Chemistry, Russian Academy of Sciences, 47 Leninsky Prosp., Moscow 119991, Russian Federation

[d]Department of Chemistry, University of Cologne, Greinstrasse 4, 50939 Cologne, Germany

*Corresponding authors.

E-mail addresses: votvagin@yandex.ru (V.F. Otvagin), irin-b@mail.ru (I.V. Balalaeva), afedorovnn@yandex.ru (A.Yu. Fedorov).

Abstract

In this report, we present a novel prodrug strategy that can significantly improve the efficiency and selectivity of combined therapy for bladder cancer. Our approach involved the synthesis of a conjugate based on a chlorin-e_6 photosensitizer and a derivative of the tyrosine kinase inhibitor cabozantinib, linked by a β-glucuronidase-responsive linker. Upon activation by β-glucuronidase, which is overproduced in various tumors and localized in lysosomes, this conjugate released both therapeutic modules within targeted cells. This activation was accompanied by the recovery of its fluorescence and the generation of reactive oxygen species. Investigation of photodynamic and dark toxicity *in vitro* revealed that the novel conjugate had an excellent safety profile and was able to inhibit tumor cells proliferation at submicromolar concentrations. Additionally, combined therapy effects were also observed in 3D models of tumor growth, demonstrating synergistic suppression through the activation of both photodynamic and targeted therapy.

Keywords: Combination Therapy, Chlorin-e_6, β-glucuronidase, Bladder cancer, Photodynamic Therapy, Cabozantinib

1. Introduction

Several decades ago, humanity entered the era of precise medicine that prompted scientists to seek advanced and selective alternatives to well-established chemotherapeutic approaches. Among the possible solutions, photodynamic therapy (PDT) has gained considerable attention due to its tissue-sparing nature and high degree of spatiotemporal control [1]. To date, PDT has been approved for the treatment of skin, head & neck, stomach, colon, bladder, brain, breast, and lung cancers [2]. Generally, PDT relies on low-toxic components: a photosensitizer (PS) and the energy from visible light. The standard treatment procedure involves intravenous administration or topical application of the PS, followed by irradiation of the tumor site. Upon exposure to light, photosensitizers generate reactive oxygen species (ROS) such as singlet oxygen - $^1O_2$ (SO), superoxide radical ($O_2^{-\cdot}$), hydrogen peroxide and hydroxyl radicals [3,4]. ROS, in turn, oxidize

nearby biomacromolecules, resulting in oxidative stress that triggers various modes of cell death [5,6]. Besides, PDT demonstrates antiangiogenic behavior [7] and belongs to a family of immunogenic treatment [8]. The latter feature is considered unique and has been exploited in numerous studies involving synergistic PDT-immunotherapy [9].

Early efforts were aimed at improving the initial photophysical properties of photosensitizers, such as ROS generation and light absorption in the NIR region (650-800 nm). Currently, researchers are focused on designing photoactive materials with advanced antitumor capabilities, as PDT still faces several drawbacks that hinder its transition to the clinic [10]. In particular, most PSs demonstrate an insufficient tumor-to-norm ratio and cause undesirable side effects in the form of photoallergic reactions as well as prolonged skin phototoxicity [11]. Besides, ROS have a limited lifetime and a short diffusion distance; therefore, the nonselective binding of PSs lowers the therapeutic potency of PDT [12]. Another "Achilles heel", known for PDT, is its oxygen-dependency, which dramatically inhibits its antiproliferative mechanisms in hypoxic tumors [13]. Moreover, the upper threshold of the phototherapeutic window is around 800 nm, within which light penetration is restricted to 1-2 mm in tissues. As a result, conventional PDT is mainly recommended for treating superficial tumors, while the irradiation of deep malignancies should be approached by utilizing optical fibers and interstitial PDT (IPDT) [14].

Recently, many strategies have been developed to overcome the aforementioned limitations. One strategy tunes PS's selectivity through the installation of various tumor-specific vectors, which include antibodies [15], peptides [16], carbohydrates [17] and low-molecular-weight ligands [18-23]. Interestingly, studies have highlighted the importance of targeting not only the cell surface but also cellular organelles during PDT [24,25]. To guarantee the effectiveness of treatment in poorly light-penetrable and hypoxic regions, combination with other therapeutic modalities, e.g., photothermal therapy [26], chemotherapy [27], and radiotherapy [28], is under intense investigation.

Despite these efforts, strategies that simultaneously address all problems are rare. In this regard, the conjugation of PSs with targeted cytotoxic agents is appealing, since it can enhance selectivity and antiproliferative behavior in a synergistic manner [29,30]. Inspired by this concept, our research group has recently synthesized and evaluated several multifunctional agents, such as **1** and **2,** based on chlorin-e_6 photosensitizers [31,32] and a well-known tyrosine kinase inhibitor (TKI) – vandetanib (Figure 1) [31-33]. By varying a design, we were able to tailor conjugated drugs **1** and **2** for a specific need, in particular, targeted delivery or combined chemo- and photodynamic therapy. It turned out that the linker's enzymatic stability is a key for the modulation of their synergistic characteristics *in vivo*. In light of these findings, we believe that next advancement can be made by employing a molecule that accumulates in tumors and simultaneously exerts an antiproliferative therapeutic effect. Herein, we report the exploration of this concept and the development of an advanced multifunctional photosensitizer for selective delivery/combinational therapy purposes.

In this work, we selected cabozantinib [34,35], a compound approved for the treatment of thyroid cancer, renal cancer and hepatocellular carcinoma, for further conjugation with chlorin derivatives (Figure 1). Several clinical trials are currently underway to evaluate the efficacy of cabozantinib in the treatment of advanced urothelial cancer including bladder cancer, alone or in combination. (NCT01688999, National Cancer Institute) [36,37]. Cabozantinib downregulates multiple receptor tyrosine kinases [38] involved in tumor progression and neoangiogenesis: c-Met (hepatocyte growth factor receptor), vascular endothelial growth factor receptor 2 (VEGFR-2), RET (rearranged during transfection), and AXL (the GAS6 receptor).

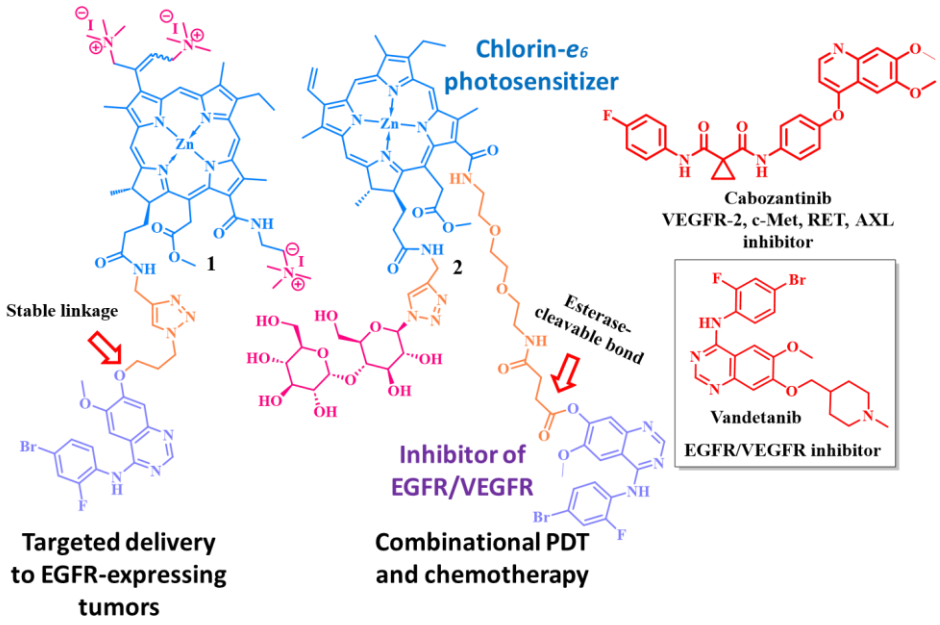

Figure 1. Structures of previously synthesized chlorin-vandetanib conjugates **1** and **2** and of the approved tyrosine kinase inhibitors (TKIs) vandetanib and cabozantinib.

In the search for an optimal conjugation strategy, we decided to incorporate a stimuli-responsive linker that would remain stable long enough to guarantee the targeted delivery of a conjugate followed by the liberation of a TKI. To this end, we have chosen a β-glucuronide linker to construct the multifunctional conjugate **3**, thereby taking advantage of the tumor's well-known ability to overproduce β-glucuronidase (Figure 2) [39]. This approach has proven effective and cancer-specific in numerous studies describing the development of β-glucuronidase-responsive prodrugs [39]. Another important factor, that prompted us to turn our attention to the β-glucuronidase prodrug approach, is the lysosome-accumulation ability of chlorin-e_6 conjugates **1** and **2** disclosed in previous studies [31,32]. As β-glucuronidase belongs to the class of lysosomal hydrolytic enzymes, it was reasonable to design the novel chlorin-e_6 conjugate **3** in accordance with its expected localization within these cellular compartments [40].

To couple chlorin and cabozantinib, we adapted the platform developed by Jeffrey et al [41,42] for the synthesis of antibody-drug conjugates (ADCs). We hypothesize that caged cabozantinib can serve as a vector to target tumor tissues by binding to tyrosine kinases. Subsequent β-glucuronidase-mediated cleavage would then trigger the simultaneous release of the

photodynamic part **4** and the cytotoxic part **5** (Figure 2). In order to improve water solubility, we implemented a straightforward approach involving the peripheral attachment of a carbohydrate [43,44]. Due to an enhanced transport of carbohydrates [45] in tumors, such a modification could potentially be beneficial for the selectivity of **3**.

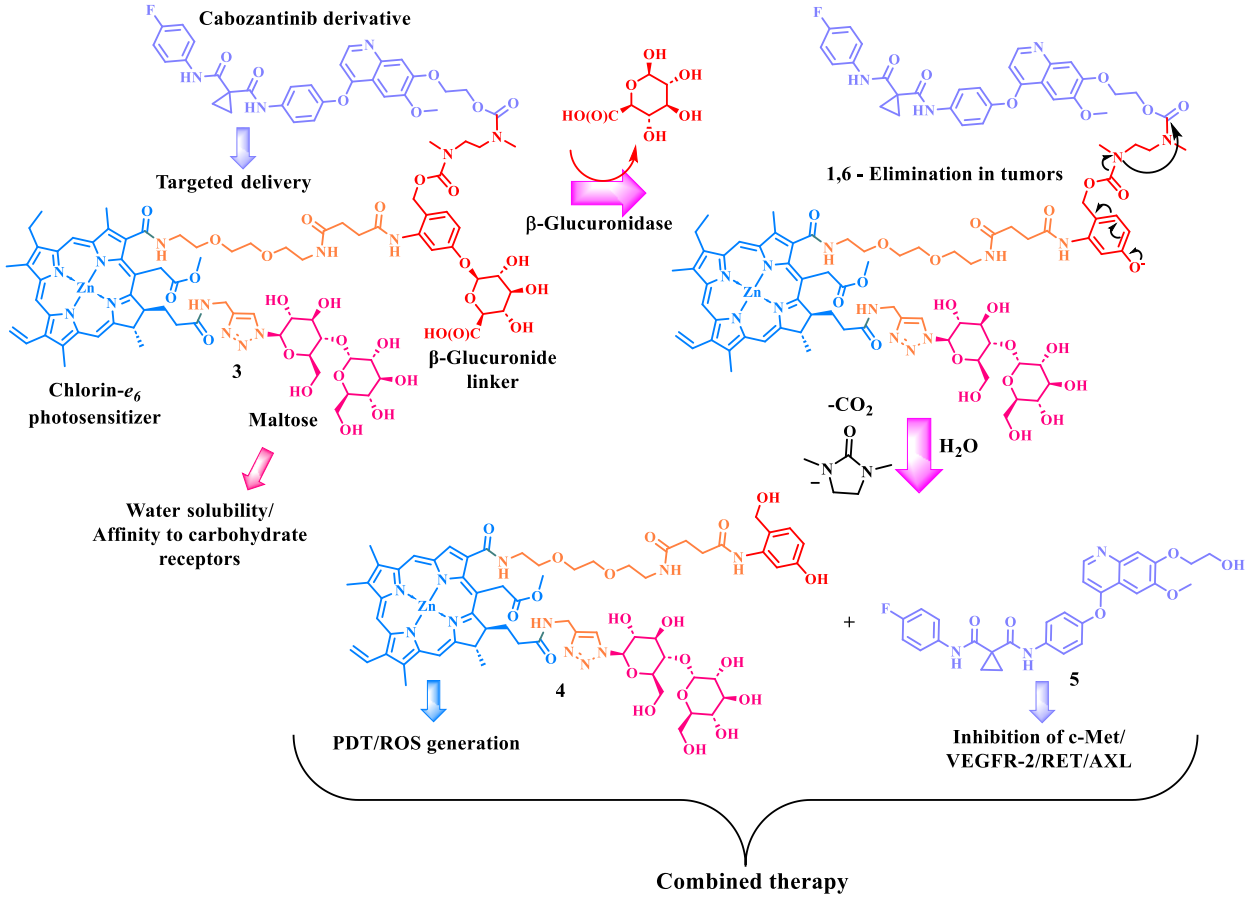

Figure 2. Structure and β-glucuronidase-mediated cleavage of proposed conjugate **3**.

Despite showing encouraging results, PDT of bladder cancers with intravenous or intravesical administration of a photosensitizer is seriously limited due to the severe adverse effects associated with the accumulation of PSs in normal urothelium [46,47]. Prodrugs, being precisely activated within tumors in a stimuli-depended manner, offer a practical solution to this problem. For example, You and colleagues have recently developed SO-cleavable prodrugs for the bladder cancer treatment [48,49]. These agents were activated by light in the presence of protoporphyrin IX and demonstrated an excellent tumor-to-norm ratio in both monolayer and 3D cell cultures. Considering these findings, we believe that the prodrug strategy deserves further investigation.

Herein, we report the synthesis of the multifunctional selective photosensitizer **3** and its evaluation for the combined treatment of bladder cancer. To our best knowledge, the conjugate **3** is the first attempt to use a β-glucuronide linker for the development of prodrugs for PDT.

2. Materials and methods

2.1. General Procedures

^{1}H NMR and ^{13}C NMR spectra were recorded on Agilent DD2 400 MHz and Bruker Avance II 600 MHz spectrometers. Chemical shifts (δ) are reported in ppm for a solution of a compound in $CDCl_3$, DMSO-d_6 or CD_3OD, with a residual peak of solvent as an internal reference, *J* values in Hertz. Mass spectra were recorded using: the MALDI method on a time-of-flight Bruker Microflex LT mass-spectrometer; the ESI (HRMS) method on a Finnigan MAT 900 spectrometer or a Bruker solariX XR 12T spectrometer. TLC analyses were carried out on Merck TLC Silica gel 60 F_{254}. Column chromatography separation was performed using Macherey-Nagel Kieselgel 60 (70-230 mesh). Purity and enzymatic cleavage of the targeted compounds was analyzed by high-performance liquid chromatography (HPLC) (Knauer Smartline S2600) using Si column (Eurospher 100-5 Si, Column 250 x 4 mm) at a flow rate of 0.4 mL/min: gradient mode from MeOH (0.1% Et_3N) / H_2O (1:9, volume ratio) to MeOH (1% Et_3N) / H_2O (9:1, volume ratio)). HPLC analysis of **5** and **26** was carried out from their PBS solutions; for conjugate **3** from PBS solution with 1% DMSO (v/v) and 5% PEG2000 (v/v). All tested compounds were found to be ≥95% pure. Commercially available reagents (Aldrich, Alfa Aesar) were used without additional purification. Solvents were purified according to the standard procedures. Petroleum ether (PE) used was of bp 40-70 °C.

2.2. Synthesis and Characterization

Conjugate (3): A 10-mL round-bottom flask was charged with a solution of the conjugate 25 (0.015 g, 0.005 mmol) in acetone (1 mL). Another 10-mL round-bottom flask was charged with $LiOH{\cdot}H_2O$ (0.005 g, 0.119 mmol) dissolved in H_2O (1 mL). The mixture from the second flask was transferred by a syringe into the first flask. The reaction mixture was stirred at 0°C for 15

min, then AcOH was added to the reaction mixture until pH = 6 followed by concentration under reduced pressure. The product was purified by column chromatography ($CHCl_3$/MeOH 80:20 to 50:50) to obtain a deep-green solid (0.008 g, 0.004 mmol, 73%). HPLC purity: 95.7%.

***N*-(4-Fluorophenyl)-*N*-(4-((7-(2-hydroxyethoxy)-6-methoxyquinolin-4-yl)oxy)phenyl)cyclopropane-1,1-dicarboxamide (5):** The THP-protected derivative **11** (0.330 g, 0.536 mmol) was placed in a flask, and dissolved in 6 mL of TFA. The reaction mixture was refluxed for 1 h, cooled, and solvent was evaporated under reduced pressure. The residue was dissolved in MeOH (5 mL), neutralized with $NH_3 \cdot H_2O$, and concentrated. The product was used without further purification (0.270 g, 0.507 mmol, 95%). HPLC purity: 95.4%.

***N*-(4-Fluorophenyl)-*N*-(4-((7-hydroxy-6-methoxyquinolin-4-yl)oxy)phenyl)cyclopropane-1,1-dicarboxamide (9):** The benzyl-protected derivative **8** (0.8 g, 1.384 mmol) was placed in a flask, and dissolved in 8 mL TFA. The reaction was refluxed for 1 h, cooled, and solvent was evaporated under reduced pressure. The residue was dissolved in MeOH (5 mL), neutralized with $NH_3 \cdot H_2O$ and concentrated. After column chromatography (EtOAc/MeOH 100:0 to 95:5), white solid was obtained (0.553 g, 1.135 mmol, 89%).

***N*-(4-Fluorophenyl)-*N*-(4-((6-methoxy-7-(2-((tetrahydro-2H-pyran-2-yl)oxy)ethoxy)quinolin -4-yl)oxy)phenyl)cyclopropane 1,1-dicarboxamide (11):** A 25-mL Schlenk flask was filled with argon and charged with **9** (0.300 g, 0.616 mmol), 2-(2-bromoethoxy)tetrahydro-2H-pyran **10** (0.386 g, 1.847) and K_2CO_3 (0.255 g, 1.847 mmol). DMF (10 mL) was added, and the mixture was stirred for 18 h at 60°C followed by concentration under reduced pressure. The residue was dissolved in EtOAc (50 mL), washed with H_2O (3 × 50 mL), dried (Na_2SO_4), and concentrated. The product was purified by column chromatography (EtOAc/MeOH 99:1 to 98:2) to obtain a white solid (0.340 g, 0.552 mmol, 90%).

2-((4-(4-(1-((4-Fluorophenyl)carbamoyl)cyclopropane-1-carboxamido)phenoxy)-6-methoxyquinolin-7-yl)oxy)ethyl (4-nitrophenyl) carbonate (12): A 25-mL flask was charged with the

alcohol **5** (0.250 g, 0.470 mmol), bis(4-nitrophenyl) carbonate (0.430 g, 1.414) and DIPEA (0.182 g, 1.410 mmol). DMF (5 mL) was added, and the mixture was stirred for 1 h at r.t. followed by concentration under reduced pressure. The residue was dissolved in EtOAc (50 mL), washed with H_2O (3 × 50 mL), dried (Na_2SO_4), and concentrated. The product was purified by column chromatography (EtOAc) to yield a white solid (0.309 g, 0.442 mmol, 94%).

***tert*-Butyl-(2-((4-(4-(1-((4-fluorophenyl)carbamoyl)cyclopropane-1-carboxamido)phenoxy)-6-methoxyquinolin-7-yl)oxy)ethyl) ethane-1,2-diylbis(methylcarbamate) (14):** A 10-mL flask was charged with the carbonate **12** (0.210 g, 0.302 mmol), *tert*-butyl methyl(2-(methylamino)ethyl)carbamate **13** (0.085 g, 0.452 mmol) and DIPEA (0.058 g, 0.450 mmol). DMF (4 mL) was added, and the mixture was stirred for 30 min at r.t. followed by concentration under reduced pressure. The residue was dissolved in EtOAc (25 mL), washed with H_2O (3 × 25 mL), dried (Na_2SO_4), and concentrated. The product was purified by column chromatography (EtOAc/MeOH 100:0 to 95:5) to obtain a white solid (0.190 g, 0.255 mmol, 84%).

2-((4-(4-(1-((4-Fluorophenyl)carbamoyl)cyclopropane-1-carboxamido)phenoxy)-6-methoxy quinolin-7-yl)oxy)ethyl methyl(2-(methylamino)ethyl)carbamate (15): The Boc-protected derivative **14** (0.069 g, 0.092 mmol) was placed in a flask, and dissolved in 3 mL DCM/TFA (1:1). The reaction was stirred for 1 h, and solvent was evaporated under reduced pressure. The residue was dissolved in DCM (25 mL), and extracted with saturated Na_2CO_3 (3 ×25 mL), dried (Na_2SO_4), and concentrated. The product was used without further purification (0.055 g, 0.085 mmol, 92%).

Methyl-1-*O*-(4-formyl-2-amino)-2,3,4-tri-*O*-acetyl-*β*-D-glucopyranuronate (18): A 50-mL flask equipped with a magnetic stirrer was charged with the methyl-1-*O*-(4-Formyl-2-nitrophenyl)-2,3,4-tri-*O*-acetyl-β-D-glucopyranuronate **17** (0.500 g, 1.035 mmol) and $SnCl_2 \cdot H_2O$ (1.170 g, 5.177 mmol). 1:1 EtOH/EtOAc (30 mL) was added, and the mixture was stirred for 2 h at 50°C followed by concentration under reduced pressure. The residue was dissolved in EtOAc (100 mL), washed with 10% NaOH (3 × 100 mL) and H_2O (100 mL), dried (Na_2SO_4), and

concentrated. The product was purified by column chromatography (EtOAc/Cy 50:50 to 70:30) to obtain a white solid (0.257 g, 0.567 mmol, 55%).

Conjugate (21): The chlorin **19** (0.300 g, 0.300 mmol) and the corresponding azide **20** (0.300 g, 0.450 mmol) were placed in a flask, and dissolved in 2:1 *t*-BuOH/$CHCl_3$ (35 mL). In another flask, $CuSO_4 \cdot 5H_2O$ (0.015 g, 0.060 mmol), TBTA (0.032 g, 0.060 mmol), AscNa (0.024 g, 0.120 mmol) were dissolved in 35 mL H_2O, and this mixture was added immediately into the *t*-BuOH/$CHCl_3$ solution in the first flask. The reaction was stirred for 1.5 h at 50 °C, cooled, solvent was evaporated under vacuum. After column chromatography ($CHCl_3$/MeOH 95:5 to 70:30), a deep-green solid was obtained (0.375 g, 0.233 mmol, 78%).

Conjugate (22): A 25-mL Schlenk flask was filled with argon and charged with the chlorin **21** (0.300 g, 0.179 mmol), and dissolved in DCM (8 mL). 2,4,6-Trichlorobenzoyl chloride (0.038 g, 0.198 mmol) and TEA (0.090 g, 0.891 mmol) were added, and the mixture was stirred for 5 h at r.t. Another 25-mL Schlenk flask filled with argon was charged with the aniline **18** (0.097 g, 0.214 mmol), DMAP (0.044 g, 0.360 mmol) and DCM (4 mL). The mixture from the second flask was transferred by a syringe into the first flask. The reaction mixture was stirred at r.t. for 19 h, then diluted with $CHCl_3$ (100 mL) and washed with H_2O (3 × 50 mL). The residue was dissolved in $CHCl_3$ (100 mL), washed with H_2O (3 × 100 mL), dried (Na_2SO_4), and concentrated. The product was purified by column chromatography ($CHCl_3$/MeOH 100:0 to 95:5) to obtain a deep-green solid (0.239 g, 0.112 mmol, 63%).

Conjugate (23): A 10-mL Schlenk flask was filled with argon and charged with benzaldehyde **22** (0.100 g, 0.049 mmol), and dissolved in $CHCl_3$/*i*-PrOH (3:1, 4 mL). Silica gel (0.200 g) and $NaBH_4$ (0.010 g, 0.263 mmol) were added, and the mixture was stirred for 1 h at 0°C. The reaction mixture was then diluted with $CHCl_3$ (20 mL), filtered through a Celite pad. The filtrate was washed with H_2O (3 × 50 mL), dried (Na_2SO_4), and concentrated. The product was purified by column chromatography ($CHCl_3$/MeOH 100:0 to 95:5) to obtain a deep-green solid (0.080 g, 0.039 mmol, 80%).

Conjugate (24): A 10-mL round-bottom flask equipped with a magnetic stirrer was charged with the benzyl alcohol **23** (0.046 g, 0.021 mmol), bis(4-nitrophenyl) carbonate (0.041 g, 0.126 mmol), and dissolved in DMF (2 mL). DIPEA (0.017 g, 0.126 mmol) was added then, and the mixture was stirred for 1 h at r.t. followed by concentration under reduced pressure. The residue was dissolved in $CHCl_3$ (25 mL), washed with H_2O (3 × 25 mL), dried (Na_2SO_4), and concentrated. The product was purified by column chromatography ($CHCl_3$/MeOH 100:0 to 95:5) to obtain a deep-green solid (0.036 g, 0.019 mmol, 89%).

Conjugate (25): The carbonate **24** (0.070 g, 0.032 mmol) and the amine **15** (0.030 g, 0.046 mmol) were placed in a round-bottom flask, and dissolved in 2 mL DMF. DIPEA (0.006 g, 0.046 mmol) was added then, and the mixture was stirred for 1 h at r.t. followed by concentration under reduced pressure. The residue was dissolved in $CHCl_3$ (50 mL), washed with H_2O (3 × 50 mL), dried (Na_2SO_4), and concentrated. The product was purified by column chromatography ($CHCl_3$/MeOH 100:0 to 93:7) to obtain a deep-green solid (0.071 g, 0.026 mmol, 81%).

Conjugate (26): A 10-mL round-bottom flask was charged with the conjugate **23** (0.025 g, 0.012 mmol), and dissolved in acetone (2 mL). Another 10-mL round-bottom flask was charged with $LiOH{\cdot}H_2O$ (0.011 g, 0.261 mmol), and dissolved in H_2O (2 mL). The mixture from the second flask was transferred by a syringe into the first flask. The reaction mixture was stirred at 0°C for 15 min, then AcOH was added to the reaction mixture until pH=6 followed by concentration under reduced pressure. The product was purified by column chromatography ($CHCl_3$/MeOH 80:20 to 50:50) to obtain a deep-green solid (0.019 g, 0.011 mmol, quantitatively). HPLC purity: 95.6%.

2.3. Determination of partition coefficients

Partition coefficients (P) were determined by adding 20 μM of the tested compounds (**3** or **26**) to 5 mL of *n*-octanol followed by addition of an equal volume of water [50]. Then, the tubes were vortexed for 1 min and placed in a shaker for 4 h at r.t. Using a centrifuge at approximately 500 g, both phases were separated and a phase containing the larger quantity of a partitioned

compound was added to a fresh aliquot of the other phase followed by the procedure described above. The experiment was repeated twice in order to stabilize the partition coefficient. The partition coefficient (P) was calculated using the following equation: $P = C_o/C_w$, where C_o – the concentration of a compound in octanol phase; C_w – the concentration of a compound in water phase.

2.4. Enzymatic cleavage of conjugate 3 and 26

Escherichia coli β-glucuronidase was purchased from Sigma–Aldrich (reference: G8295). The conjugate **3** or the chlorin **26** (0.1 mg/mL) was incubated with E. coli β-glucuronidase (200 U/mL) in a phosphate buffered saline (PBS, 0.02 M, pH 7.4) with 1% DMSO (v/v) and 5% PEG2000 (v/v) at 37 °C. Aliquots of 40 μL were taken at indicated time and analyzed by HPLC. The retention times for compounds conjugate **3**, chlorin **4** and cabozantinib derivative **5** were 28.0, 26.2 and 39.4 min respectively.

2.5. Photophysical measurements

The conjugate **3** or the chlorin **26** were dissolved in DMSO/PEG2000/dH_2O (5:10:85, v/v) at 1 mM (stock solutions). For measuring the photophysical properties and cell studies, the stock solutions were further diluted with deionized water.

Absorption and fluorescence spectra were registered using a Synergy MX spectrophotometer-spectrofluorometer (BioTek, USA). Fluorescence was excited at 410 nm.

The molar extinction coefficient ε was determined using the following equation:

$$\varepsilon = {}^{D}/_{cl} \ ,$$

where D is the optical density; l is the path length; and c is concentration.

The fluorescence quantum yield φ_1 was calculated using the equation:

$$\varphi_1 = \frac{\varphi_2 F_1 D_2}{F_2 D_1} \ ,$$

where F_1 and D_1 are the integral fluorescence intensity and the optical density of **3** (or **26**), respectively; φ_2 is the quantum yield of Rhodamine B (Sigma, USA) in water (0.31); F_2 and D_2 are the integral fluorescence intensity and the optical density of Rhodamine B, respectively.

The optical density was measured at 410 nm; the fluorescence was excited at the same wavelength was and detected at 550–850 nm.

2.6. Singlet oxygen generation experiments

1,3-Diphenylisobenzofuran (DPBF) was used as the singlet oxygen sensitive trap. A reaction medium containing 100μM DPBF and 10 nM **3** or **26** in DMSO was irradiated using the LED a light source (655−675 nm, 32 mW/cm^2) [51] in doses up to 5 J/cm^2 with 0.5 J/cm^2 step. DPBF bleaching during the photoinduced reaction was registered at every step using a Synergy MX spectrophotometer. Quantum yields of the singlet oxygen generation (Φ_Δ) were determined for the first linear stage of the DPBF bleaching by a comparative method using the following equation:

$$\Phi_{\Delta 1} = \Phi_{\Delta 2} \frac{(D_0 - D)_1}{(D_0 - D)_2}$$

where $\Phi_{\Delta 1}$ is the quantum yield of the analyzed compound, $\Phi_{\Delta 2}$ is the quantum yield of Photodithazine® used as a reference [0.56] [52], D_0 and D are the optical density at 420 nm before and after irradiation at dose 1 J/cm^2.

2.7. Cell line and culturing conditions

Cells of the human urinary bladder transitional cell carcinoma T-24 line (obtained from Russian Collection of Cell Cultures of Vertebrates) were cultured in Eagle's minimum essential medium (MEM) (PanEco, Russia) with 10% (v/v) fetal calf serum (HyClone) and L-glutamine in 5% CO_2 at 37 °C. At each passaging stage, the cells were treated with trypsin-ethylenediaminetetraacetic acid (EDTA) (1:1) solution (PanEco, Russia).

2.8. Generation of a fluorescent tumor cell line

To obtain a stable fluorescent tumor cell line, the parental T-24 cells were transfected by lipofection technique with mammalian expression vector pTagGFP2-N (Evrogen) encoding green fluorescent protein TagGFP2 using Fugene (Roche, USA) transfection reagent according to the manufacturer's protocols. Transfectants were primarily selected on the medium with increasing concentrations up to 2mg/ml of G418 antibiotic (Sigma), and then transfected cells were sorted using a FACS Aria III cell sorter (BD Biosciences, USA). The fluorescence of TagGFP2 was excited at 488 nm and recorded at 515-545 nm. Cells were sorted, expanded in cell culture and sorted again to obtain the brightest fluorescent cell subset, with three sort/expansions cycles. At the last step, the single cell sorting was performed, and the cell clones were expanded from individual cells. The obtained monoclonal cell line, selected based on its fluorescent and growth parameters and named T-24-GFPcyto, was maintained in the same way as parental T-24 cells.

TagGFP2 expression and localization in created cell line was confirmed using a laser scanning confocal microscope Axio Observer Z1 LSM 710 NLO/Duo (Carl Zeiss, Germany). The images were obtained with C-Apochromat 63× water immersion objective lens with numerical aperture 1.2. The fluorescence of TagGFP2 protein was excited at 488 nm and collected in the range of 500-560 nm.

2.9. Study of cellular uptake of the tested compounds

The cells were seeded in a 96-well plate (Corning) at the density 5×10^3 cells per well and allowed to attach overnight. Then, the medium was exchanged with fresh serum-free growth medium containing 5 μM of a tested compound (200 μL per well) and the cells were incubated for 24 h. After incubation and medium exchange to fresh one without compounds, the cells were stained with the following organelle-specific dyes according to the manufacturer's instructions (Thermo Fisher Scientific): 0.5 μM LysoTracker Green DND-26, 0.5 μM MitoTracker Green FM, 0.5 μM ER-Tracker, 5 μM BODIPY FL C5-ceramide complexed to BSA for the Golgi apparatus, and 1X working solution CellMask Plasma Membrane Green Stain.

Colocalization of the tested compounds and organelle-specific dyes was analyzed using a laser scanning confocal microscope Axio Observer Z1 LSM 710 NLO/Duo. Fluorescence of stained organelles was excited at 488 nm and recorded in the range of 500−550 nm; fluorescence of the compounds was excited at 633 nm and recorded at 650−735 nm.

Semi-quantitative analysis of the compounds' fluorescence intensity was performed using the ZEN 2012 program; at least 10 cells in two to three fields of view were analyzed.

2.10. Cytotoxicity study

The effect of tested compounds on cell viability was estimated using the microculture tetrazoline test (MTT) [53]. Cells were seeded in 96-well plates at the density of 4×10^3 cells per well and allowed to attach overnight. The medium was then exchanged with fresh serum-free growth medium containing tested compounds in varying concentrations. After 24 h incubation, the medium was exchanged with full fresh growth medium. To estimate the photoinduced toxicity of the tested compound, we exposed the cells to light irradiation (655−675 nm, 32 mW/cm^2, 20 J/cm^2) using a LED light source [51]. Irradiated cells were then incubated for 24 h before cell viability was measured. For this, the cells were incubated with serum-free medium containing 0.5 mg/mL MTT reagent [3-(4,5-dimethyl-2-thiazolyl)-2,5-diphenyl-2H-tetrazole bromide, Alfa Aesar, U.K.] for 4 h. The formazan formed from the reduction of MTT by cell dehydrogenases was dissolved in DMSO, and the absorbance was measured at 570 nm with a Synergy MX plate reader.

The same procedure was performed for the estimation of the dark toxicity of the conjugates, except for that there was no cell exposure to LED light.

Cell viability was expressed as the ratio of the optical density of treated and untreated cells (in percentage). Three independent experiments (all in triplicate) were performed. Data analysis and calculation of half-maximal inhibition concentration IC_{50} were performed using the GraphPad Prism 6 software and a four-parameter model for the lognormal distribution.

2.11. Determination of the combination index

Combination index (CI) was calculated using the following formula:

$$CI = \frac{D_1}{DX_1} + \frac{D_1}{DX_2}$$

where D_1 is IC_{50} for conjugate **3**; DX_1 and DX_2 are IC_{50} of individual **26** and **5** respectively. Combination index defines relationships between modules in conjugated drugs and indicates synergism (CI < 1), additive effect (CI = 1) or antagonism (CI > 1).

2.12. Fluorescence-based Cytotoxicity Study in Collagen Hydrogel

Human urinary bladder carcinoma T-24 line is non-tumorigenic in immunocompromised mice and cannot be used in xenograft models. Thus, to analyze the cell response to treatment in complex tissue-like conditions, we used matrix-based 3D in vitro model of tumor growth.

The fluorescent T-24-GFPcyto cells were embedded in collagen type I hydrogel, prepared as previously described[71] with volume density of 2×10^5 cells per mL in a 6-well culture plate. The tested compounds were added to the culture medium 72 h after the cell embedment when the 3D culture was completely formed. The treatment concentrations of the tested compounds were equal to IC_{50}, $5\times IC_{50}$ and 10×IC50 of **3** for monolayer cell culture. After 24 h incubation, the medium was exchanged to fresh full medium and the hydrogels were irradiated as described above. The growth of cells culture and its response to treatment was analyzed daily using fluorescence registration with DVS-03 fluorescence macroimager (Institute of Photonic Technologies of the Russian Academy of Sciences, Moscow, Russia). The fluorescent images of the gels were acquired with excitation at 490 nm and emission registration at 513-556 nm; the images were proceeded and analyzed using ImageJ software (version 1.50i, National Institute of Health, Bethesda, Maryland, USA) as described previously [54].

3. Results

3.1. Chemistry

Starting from commercially available apocynin **6** and 1,2-cyclopropanedicarboxylic acid **7**, the benzyl-protected derivative of cabozantinib **8** was obtained according to the known procedure

[55] (Scheme 1). Further deprotection of the benzyl group in boiling TFA gave compound **9** in 82% yield.

Scheme 1. Synthesis of c-Met ligand **9**.

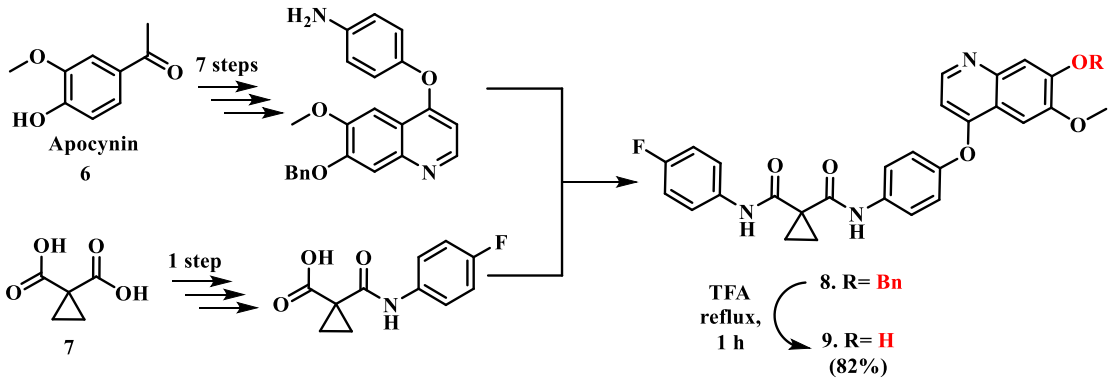

To diminish a steric hindrance and improve binding to receptor kinases, we coupled a short linker **10**, obtained from ethylene glycol [56], with **9** via alkylation and synthesized THP-protected cabozantinib derivative **11** in 75% yield (Scheme 2). The next step involved deprotection of **11** in acidic media in 86% yield with subsequent transformation of the resulting alcohol **5** into carbonate **12** in a near quantitative yield. The reaction of **12** with mono-Boc-protected diamine **13** led to carbamate **14**, and further removal of the Boc-group furnished the chemotherapeutic building block **15** in a high yield.

Scheme 2. Synthesis of chemotherapeutic building block **15**.

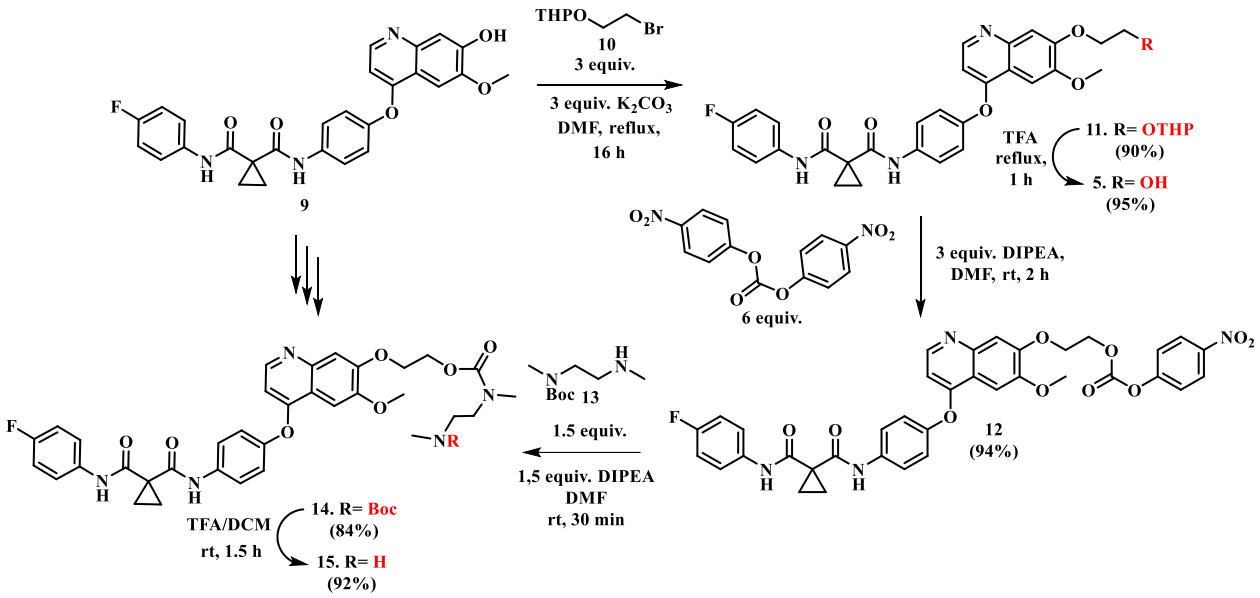

D-(+)-Glucuronolactone **16**, a widespread food additive [57], was converted into the nitro-containing ether **17** in 3 steps according to well-known protocols for the synthesis of β-glucuronide linkers [58] (Scheme 3). Following $SnCl_2$-mediated reduction of **17** gave the aniline derivative **18** in 55% yield. In order to obtain the photosensitizing counterpart, we exploited the previously developed synthetic route including a 4-step synthesis of bifunctional chlorin-e_6 derivative **19** from naturally occurring MePheid-*a* [32]. Then, the alkyne-containing compound **19** was subjected to Cu (I)-catalyzed azide-alkyne cycloaddition (CuAAC) with the azido-substituted maltose heptaacetate **20** [32] leading to the glycoconjugate **21** in 78% yield. The key conjugation step involved a Yamaguchi-type amidation reaction of **21** in the presence of the aniline derivative **18** via activation of the carboxylic moiety by TCBC (2,4,6-trichlorobenzoyl chloride, Yamaguchi reagent) to afford the corresponding derivative **22** in 45% yield. Next steps were aimed at the creation of a required conjugation site in **22**, which was achieved by high-yielding step-by-step reduction of its aldehyde moiety to give the benzylic alcohol **23** in 80% yield. Finally, the reaction of **23** with bis(4-nitrophenyl) carbonate furnished the carbonate **24** in 89% yield, which was ready for coupling with the chemotherapeutic building block.

Scheme 3. Synthesis of the β-glucuronide linker **18** and the photoactive building block **21** followed by their conjugation.

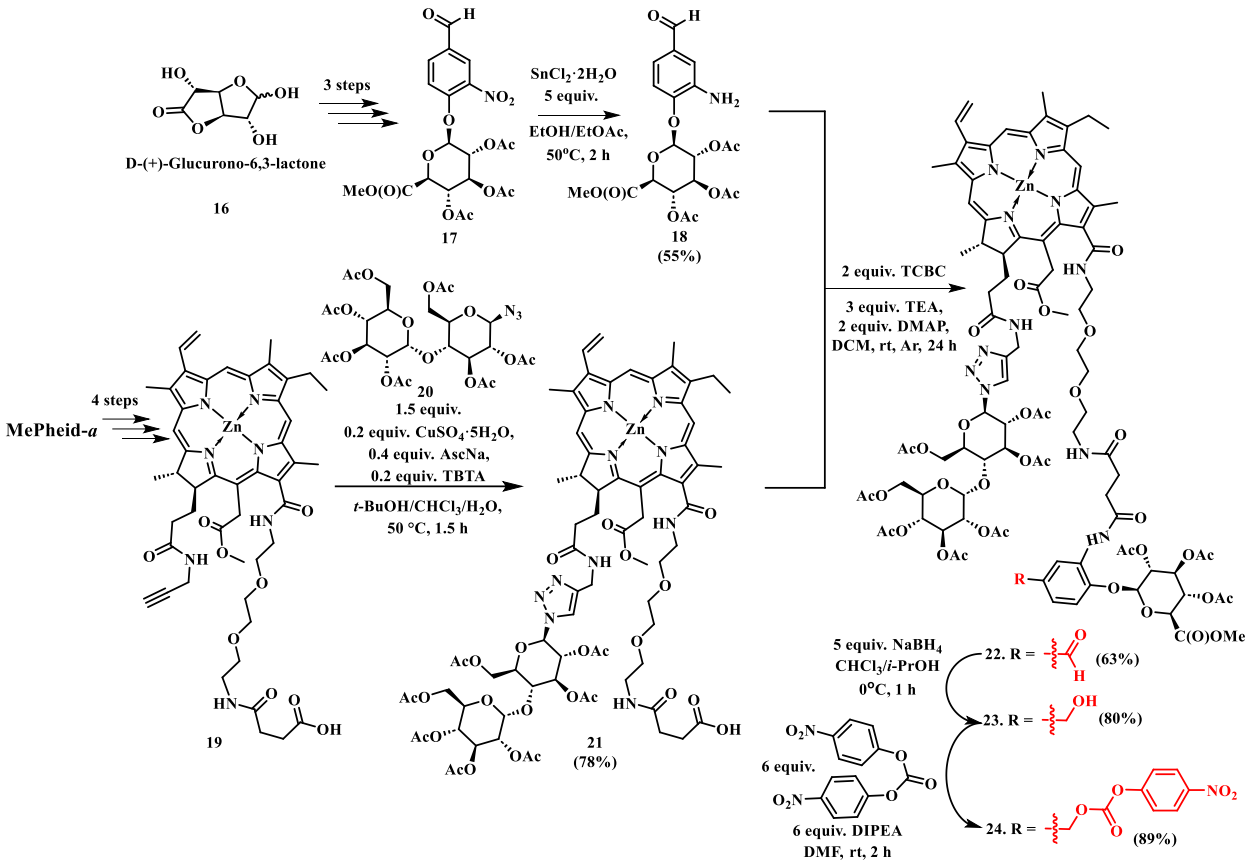

The conjugation of the obtained building blocks **24** and **15** proceeded smoothly in DMF giving conjugate **25** in 81% yield. After removal of all 11 protective groups under basic conditions, the target conjugate **3** was obtained in 73% yield (Scheme 4A). One common approach to evaluate biological properties of combined drugs is a comparative analysis of the unconjugated drugs (reference) and the conjugated analog. Therefore, we subjected derivative **23** to hydrolysis to obtain the glycosylated chlorin **26** in quantitative yield as a reference for further investigations (Scheme 4B).

Scheme 4. (a) Synthesis of the target conjugate **3**. (b) Synthesis of reference photosensitizer **26**.

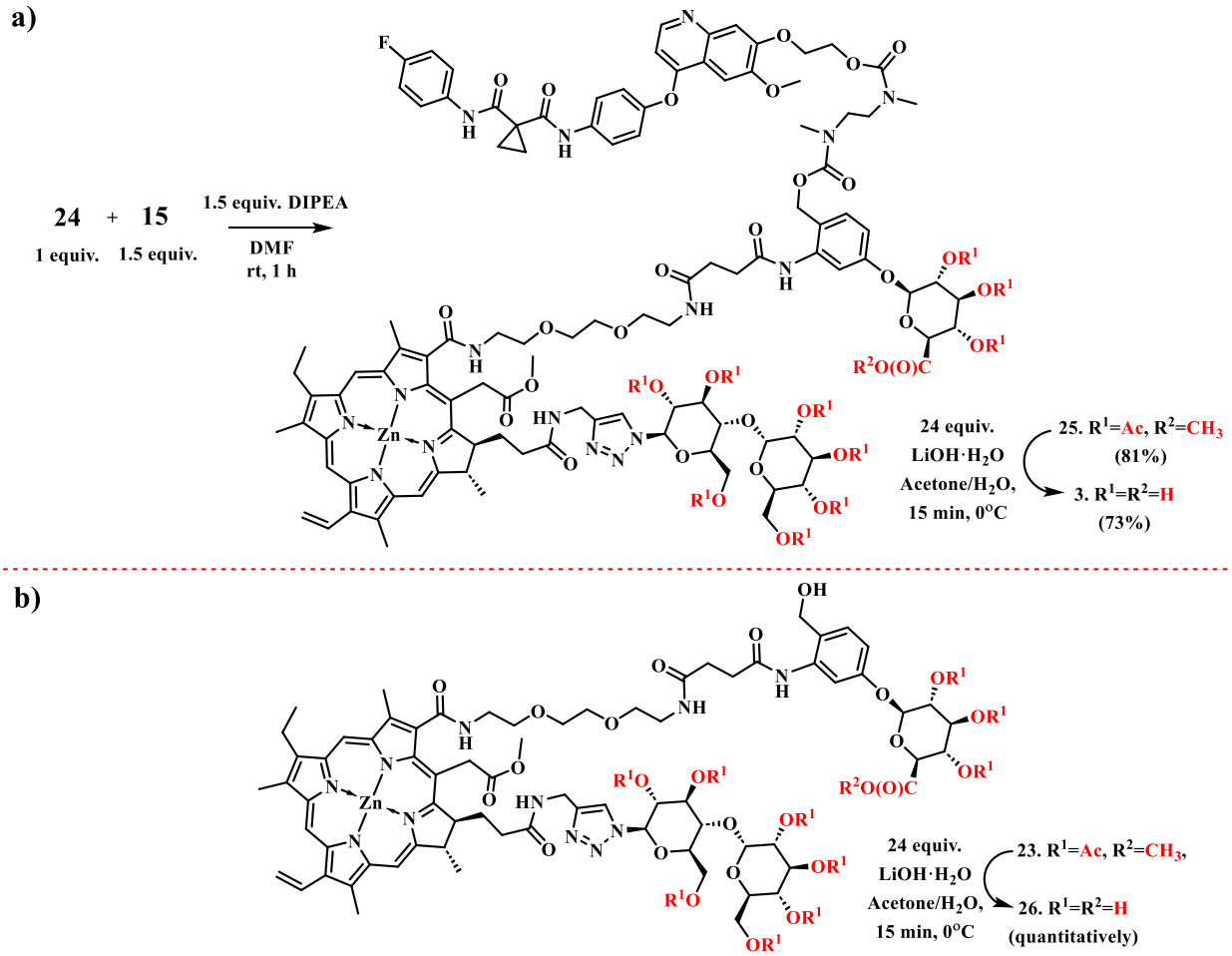

Although the synthesized conjugate **3** carried a considerable number of hydrophilic moieties, its solubility in water still remained insufficient due to time-dependent aggregation behavior. Chlorin **26**, on the contrary, demonstrated less pronounced aggregation. To ensure water solubility, we used the common solubilizer PEG2000 [59] and prepared stock solutions (mM) of **3** or **26** in DMSO/PEG2000/H_2O (5:10:85, v/v), which were then diluted to yield μM solutions with following concentrations of additives: 0.025% DMSO (v/v) and 0.05% PEG2000 (v/v). Monitoring of possible aggregation was carried out spectrophotometrically (discussed below). Evaluation of the partition coefficient in a *n*-octanol/water system indicated comparatively high lipophilicity for the conjugate **3** (logP = 1.37), while the glycosylated chlorin **26**, lacking the lipophilic chemotherapeutic part, was clearly hydrophilic (logP = -0.35). The hydrophilic/lipophilic balance of the PS determines a wide range of pharmacological properties including tumor uptake, intracellular localization and membrane penetration [60]. Despite the

fact, that administration of **3** requires complex formulations, its logP is within the optimal range (logP ~ 1-3) for therapeutic agents [61] which may improve druglikeness.

3.2. Photophysical and β-glucuronidase responsive properties

The electronic absorption spectra of **3** and **26** were recorded in DMSO/PEG2000/H_2O solutions, where they showed sharp and intense Soret and Q bands at 648/642 nm and 416/412 nm, respectively (Table 1, Figure 3a). Upon excitation at 410 nm, the conjugate **3** was almost nonfluorescent with a fluorescence quantum yield (Φ_F) of 0.1 %. By contrast, the reference chlorin **26** demonstrated brighter fluorescence with Φ_F = 1.2%. To probe whether the fluorescence quenching of **3** was related to the presence of the cabozantinib moiety, we added external β-glucuronidase to its PBS solution. As a result, the gradual increase of fluorescence was observed indicating the enzymatic cleavage of the β-glucuronide linker followed by the liberation of **5** (Figure 3b). Since no obvious concurrent energy or electron transfer process exists in the case of the chlorin-cabozantinib dyad **3**, we assumed that aggregation, a well-known feature of porphyrinoid PSs, might interfere with the emission. However, the absorbance spectra of **3**, recorded at concentrations up to 10 μM, correlated with the Beer–Lambert law and did not indicate a J- or H-aggregate formation via a peak shifting (Figure 3c). Probably, the conjugate **3** participated in another self-assembling pattern. The similar quenching was also reported by Huang during the investigation of the cleavable phthalocyanine-tetrapeptide-doxorubicin conjugate [62]. In principle, the fluorescence signal of **3** can be used to monitor its cleavage in tissues with different levels of β-glucuronidase.

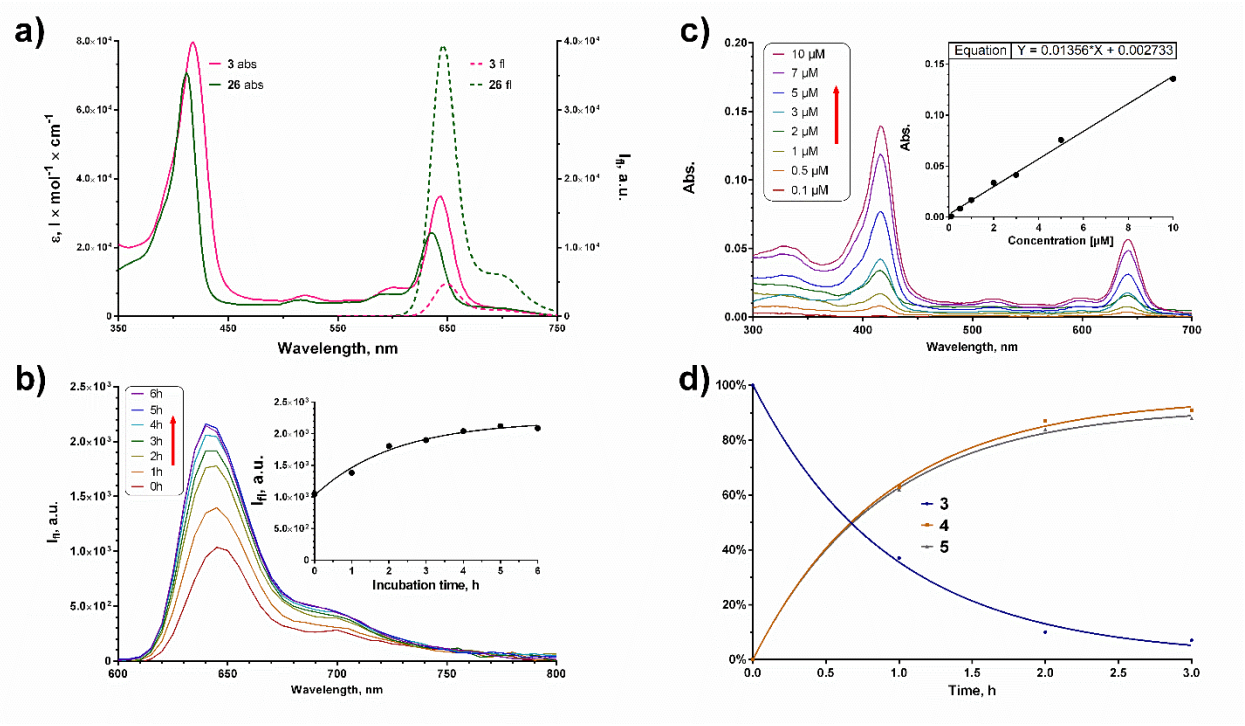

Figure 3. (a) UV-Vis absorption and fluorescence (λ_{ex} = 410 nm) spectra of **3** and **26** (both at 5 μM) in water with 0.025% DMSO (v/v) and 0.05% PEG2000 (v/v); (b) Change in the fluorescence (λ_{ex} = 410 nm) spectra of **3** (5 μM) in PBS with 0.025% DMSO (v/v) and 0.05% PEG2000 (v/v) in the presence of 40 U/mL β-glucuronidase over 6 h (37 °C); (c) Change in the electronic absorption of **3** at different concentrations; (d) Enzymatic cleavage of the conjugate **3** (0.1 mg/mL) in the presence of β-glucuronidase (200 U/mL) monitored by HPLC.

Table 1. Photophysical characterization of compounds **3** and **26**.

Compound	λ_{abs} (nm) / log ε	λ_{em}[a] (nm)	Φ_F[b] (%)	Φ_Δ[c] (%)
3	416 / 4.7	648	0.1	5
	642 / 4.3			14 (+β-glucuronidase)
26	412 / 4.5	646	1.2	5
	636 / 3.9			29 (+β-glucuronidase)

[a]Excited at 410 nm. [b]Relative to Rhodamine B in water. [c]Determined using DPBF as a chemical trap (relative to Photoditazine®).

The singlet oxygen (SO) generation quantum yield (Φ_Δ), an important parameter for a photosensitizing drug, was determined for **3** and **26** using 1,3-diphenylisobenzofuran (DPBF) as

the ROS scavenger (Table 1). The solution of Photoditazine® in DMSO was used as a standard (for details see Experimental Part). Both molecules generated SO with Φ_Δ = 5% in DMSO solutions which were ca. 5 times lower than that of the conjugate **2** measured in our previous work [32] (Figure 1). Further addition of β-glucuronidase deblocked the photo-induced generation of SO for the conjugate **3** yielding Φ_Δ =14%. Similarly, the SO generation quantum yield was restored (Φ_Δ = 29%) for the reference chlorin **26**. As a possible explanation, the glucuronic moiety, being detached from the investigated chlorins, might be responsible for their association resulting in the fluorescence and SO generation inhibition. In our opinion, the observed quenching pattern can be exceptionally beneficial since the activation of conjugate **3** should preferably take place in a β-glucuronidase-rich environment, *i.e.*, in tumor tissues. In addition, we carried out photobleaching experiments for both compounds during which the conjugate **3** demonstrated greater stability under irradiation (Figure S46).

Finally, we quantitatively evaluated the enzymatic cleavage of **3** and **26** by means of HPLC (Figure 3d, Figure S44, Figure S45). After addition of β-glucuronidase, both molecules released a chlorin derivative with identical Rt and UV-Vis spectra, which was attributed to the formation of the chlorin **4**, while the conjugate **3** also demonstrated liberation of the cabozantinib derivative **5** in a time-dependent manner.

3.3. Cellular uptake study

Having investigated β-glucuronidase responsive properties for the synthesized conjugates, we set out to explore their ability to be accumulated by the living cells, namely, T-24 (Human urinary bladder carcinoma). Up-regulation of c-Met is involved in bladder cancer progression and reported in T-24 cells [63]. In this regard, PDT accompanied with the c-Met inhibition via **5**, liberating during treatment, might be advantageous for the therapeutic outcome.

At first, we demonstrated that PEG2000 and DMSO additives were non-toxic in a broad range of concentrations (Figure S48). Then, using flow cytometry with immunofluorescence staining, we proved that T-24 cells, indeed, express c-Met (Figure S47). In accumulation experiments

fluorescence signal of the chlorins **3** and **26** was detected in the perinuclear region indicating successful uptake by T-24 cells (Figure 4a). As the fluorescence of **3** at maximum was ca. 4-5 times stronger (Figure 4b), it can be concluded that the intracellular concentration of **3** is significantly higher than that of **26**. The latter observation might be due to higher affinity of **3** toward c-Met expressing T-24 cells as well as higher lipophilicity facilitating transportation of **3** through a lipid bilayer. As cabozantinib reverses the ABCG2-mediated multidrug resistance [64] and chlorin-e_6 photosensitizers are known ABCG2 substrates [65], we speculate that the increased cellular uptake of **3** is provoked by the cabozantinib moiety antagonizing its efflux.

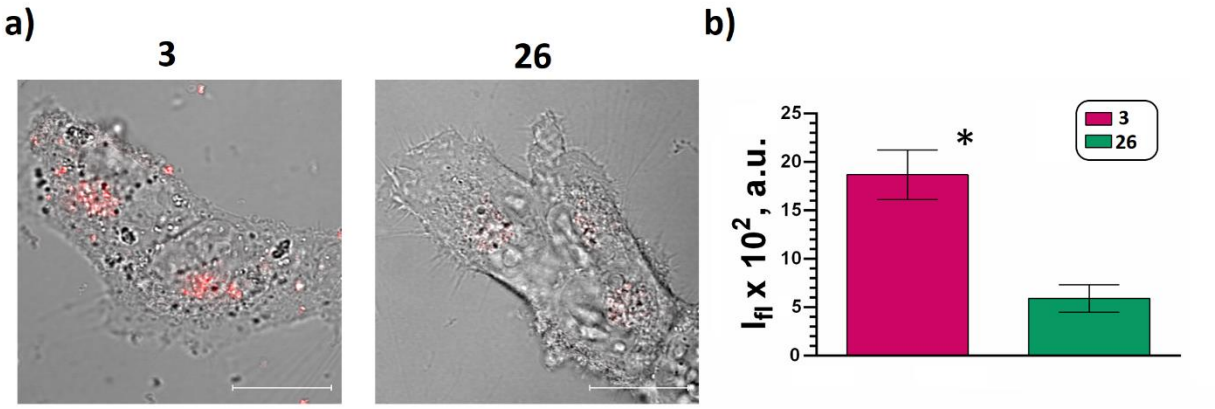

Figure 4. Cellular uptake study of **3** and **26** by T-24 cells. (a) Confocal images of the living cells after 24 h incubation in the serum-free growth medium containing 5 μM of a tested compound, the merged images in transmitted light and red fluorescence are shown, bar is 20 μm. (b) Results of the qualitative analysis of the cellular fluorescence signal. At least ten cells in two-three fields of view were analyzed; means ± SD.

The co-localization analysis with dyes, specific to particular cellular organelles, demonstrated that both compounds were mainly localized in lysosomes and other vesicles in living cells; much fewer amounts of the compounds were observed in ER and Golgi Apparatus (Figure 5). That allowed us to assume the active ATP-dependent endocytosis for **3** and **26**, which was also proposed for the structurally similar conjugate **2** in our previous studies [32] (Figure 1). It should be noted, that lysosome targeting is an important paradigm to improve PDT efficiency [66,67], therefore the pronounced localization of the conjugate **3** in these vesicles might be highly

beneficial. The PDT-mediated disintegration of lysosomal membrane leads to the cytoplasmic release of metal ions and hydrolases triggering cell death including catepsin-, calpain-, and calcium-dependent pathways [68]. Besides, we expect efficient activation of the prodrug **3** in cells, since β-glucuronidase is a member of lysosomal enzymes family [40].

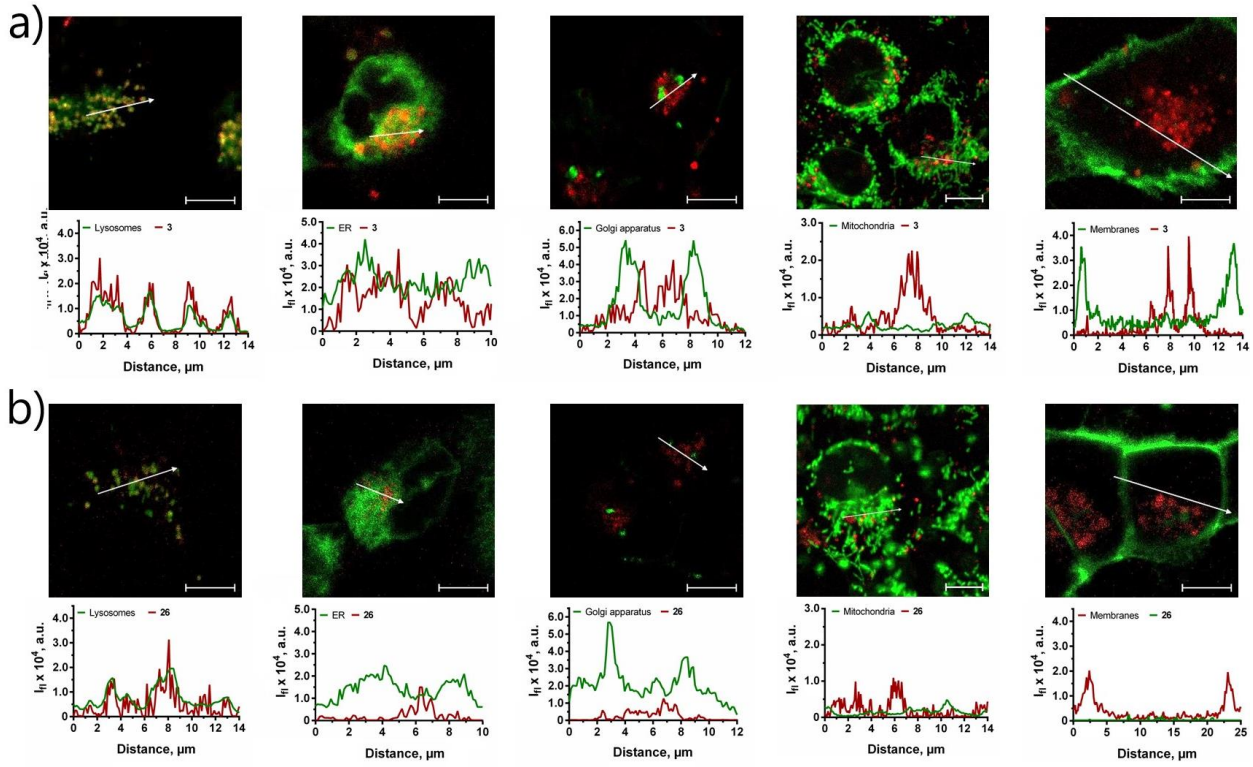

Figure 5. Analysis of intracellular localization of **3** (a) and **26** (b) in T-24 cells. The cells were incubated with the compounds (5 μM) for 24 hours and then stained with the following dyes: LysoTracker Green for lysosomes; LysoTracker Green for mitochondria; ER-Tracker for ER and BODYPY FL C5-ceramide complexed to BSA for Golgi apparatus; CellMask™ Plasma Membrane Stains for the cell membrane. The merged fluorescent channels are presented; fluorescence signal profiles are shown along the lines indicated by the white arrow on the images. Scale bars: 10 μm.

3.4. Photodynamic activity in monolayer cell culture

Both dark toxicity and photodynamic activity of **3** and the reference compound **26** were compared against T24 cells in a monolayer culture. In dark experiments, the compounds exhibited toxic properties at concentrations above 10 μM (24 h incubation, Fig. 6, Table 2).

However, the measured IC_{50} index for the conjugate **3** was 77 μM indicating lesser antiproliferation activity. Under irradiation (20 J/cm^2), the cells viability was pronouncedly reduced even when treated with 0.01 μM of **3**, and $IC_{50\ light}$ was calculated at about 0.2 μM. The photodynamic index of more than 380 demonstrated an excellent balance between photo-induced and dark cytotoxicity for **3**. On a contrary, the photodynamic activity of **26** was one order of magnitude lower ($IC_{50\ light}$ 3.3 μM), than that of **3**, which was clearly due to its hindered cellular uptake. The latter assumption was supported by the observation that pre-incubation with **3** in the presence of β-glucuronidase resulted in significant reduction of its toxicity which became equal to that of **26**.

Table 2. *In vitro* light and dark cytotoxic activity of **3** and **26**.

	$IC_{50\ Dark}$, μM	**$IC_{50\ Light}$, μM**	**$IC_{50\ Dark}$/ $IC_{50\ Light}$**
3	76.87 [60.72-97.3]	0.2 [0.13-0.33]	~384
3 +β-glucuronidase	36,55* [29.32-45.56]	3,8 [1.42-7.68]	~10
26	45.44* [35.98-57.38]	3.3* [1.04-4.89]	~14

* – statistically significant difference from **3** ($p<0.01$, *t*-test)

Table 3. *In vitro* cytotoxic activity of **5**.

	$IC_{50\ 24h}$	**$IC_{50\ 72h}$**
5	1.2 [0.97-1.6]	0.4* [0.24-0.7]

* – statistically significant difference from **$IC_{50\ 24h}$** ($p<0.01$, *t*-test)

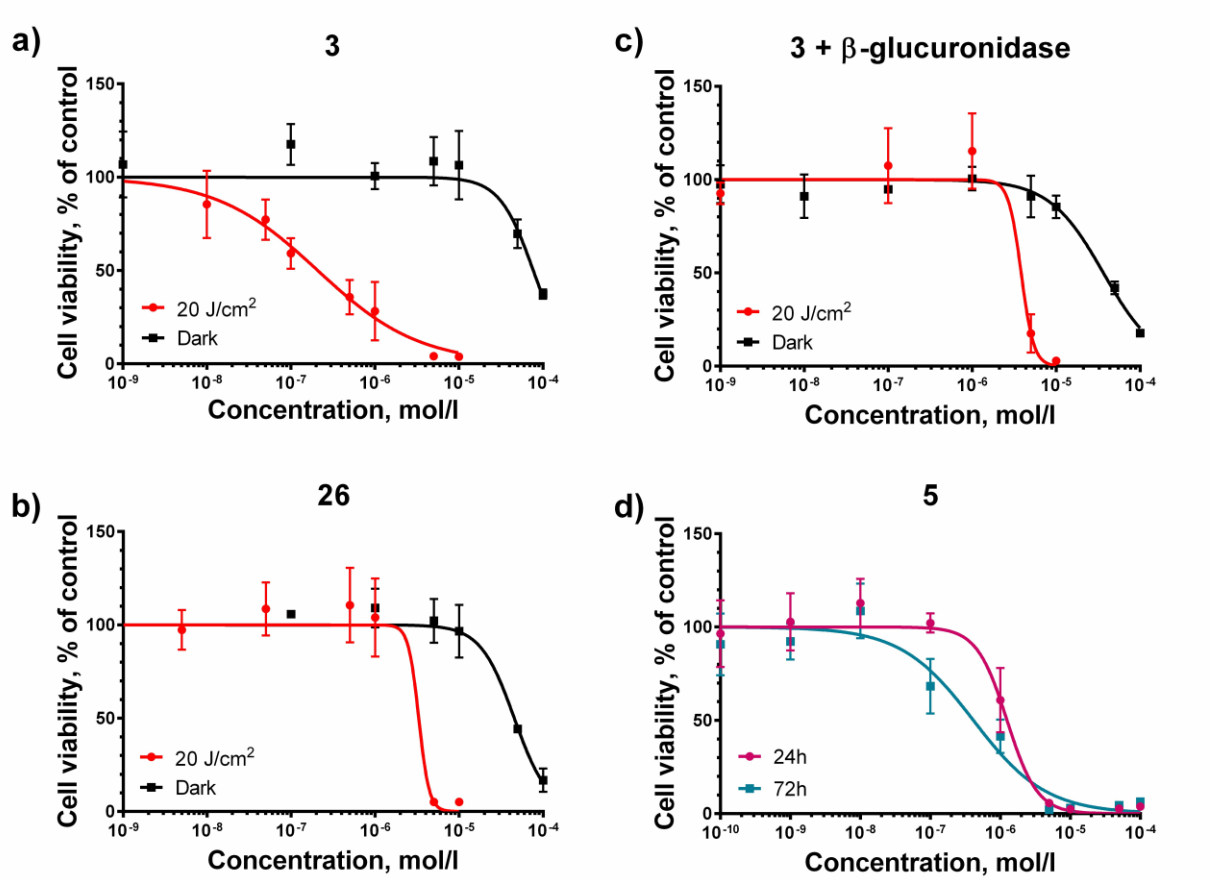

Figure 6. Relative viability of T-24 cells treated with **3** (a), **26** (b), **3**+β-glucuronidase (c) and **5** (d) in dark or under light exposure. Cells were incubated with the compounds **3** and **26** for 24 h; with **5** for 24 or 72 h; β-glucuronidase was added simultaneously with **3**, the medium was exchanged with full fresh growth medium, and the cells were irradiated in dose 20 J/cm^2 (λ = 655-675 nm, power 32 mW/cm^2) or stayed in dark. After the additional incubation for 24 h, cell viability was measured by MTT-assay and expressed as the percentage to untreated cells. Means ± SD are presented; the experimental data are fitted using four parameters model for the lognormal distribution.

The cabozantinib derivative **5** alone showed time-dependent inhibition of T24 cells proliferation with IC_{50} of 1.2 μM and 0.4 μM after 24 and 72 hours of the incubation respectively (Table 3, Figure 6d). Obtained numbers were consistent with previously reported data on the inhibitory activity of cabozantinib [69]. While PDT belongs to cytotoxic treatment, the cabozantinib activity is based on a blockage of the mitogenic signaling and the cytostatic arrest

of cellular proliferation with long-term therapeutic effects. To determine the type of drug interaction for two active counterparts in the conjugate **3**, the combination index (CI) [70] was calculated. The obtained CI value of 0.23 suggested a strong synergism between photodynamic and targeted modules highlighting potential benefits associated with the utilization of the developed conjugated platform.

3.5. Anticancer efficiency in 3D *in vitro* model of tumor growth

The response of cancer cells to treatment and their potential to develop drug resistance strongly depends on the particular microenvironment, which includes factors such as the presence of extracellular matrix and the spatial organization of the experimental "tumor" [71-73]. However, the human urinary bladder carcinoma T-24 cell line demonstrates limited capability to form tumor nodes when introduced into immunocompromised mice [74,75]. This fact motivated us to establish a 3D matrix-based *in vitro* model to comprehensively assess the efficiency of the conjugate **3.** To monitor cell culture growth under various treatment conditions, we employed a non-invasive fluorescence macro-imaging approach [76,54].

At first, we created a stable population of fluorescent urinary bladder carcinoma cells (designated as T-24-GFP-cyto cells) expressing the TagGFP2 protein. This cellular line was obtained by lipofection technique, followed by repeated cycles of optical sorting and culture expansion. The monoclonal cell line was established via single-cell sorting, specifically selecting the highly fluorescent clone that exhibited growth characteristics similar to those of the parental T-24 cell line. The TagGFP2 protein was evenly distributed within the cytoplasm and nuclei of the cells, thus providing a bright green fluorescence signal of T-24-GFP-cyto monoclonal cell line with narrow distribution across the cell population (Fig. 7a). The transfection stability was verified by the persistent TagGFP2 fluorescence observed over at least 20 passages and even during the cryopreservation of the cell culture.

The resulting T-24-GFP-cyto cells were embedded in a collagen hydrogel, which allowed the cells to move freely in a three-dimensional space and form cell conglomerates with a

corresponding communication network. The total amount of the fluorescent cells in a matrix volume was measured by daily fluorescence imaging of the gels without destruction or impairing their structure (Fig. 7b) [54].

The cells were allowed to grow continuously within the 3D matrix for a duration of 8 days under observation (Fig. 7c). Upon the addition of the conjugate **3** to the medium, followed by the irradiation of the gels in 24 h, resulted in a pronounced dose-dependent inhibition of culture growth. As expected, the resistance of cells to treatment, when embedded in 3D matrix, significantly surpassed that observed in a monolayer culture. Even the $10\times IC_{50}$ concentration, calculated for the monolayer, led to the death of only about a half of cell population in hydrogel (Fig. 7c, 7d). Additionally, 4 days after PDT treatment, the culture's growth was significantly recovered. Similar resistance of malignant cells to treatment with chemo-, photodynamic-, or targeted therapeutics in a tissue or tissue-like microenvironment has been observed in various studies [77-79], presenting a major challenge in the translation of candidate drugs to clinics. To prove the role of the cabozantinib moiety in anticancer effect of the conjugate **3**, we compared the growth-inhibition activity of **3** and **26** (Fig. 7d). One day after PDT, the effect of treatment with $10\times IC_{50}$ of **26** was comparable to that of $10\times IC_{50}$ of **3**. Unlike conjugate **3**, the chlorin **26** had a short-term antitumor effect, and in two days (3 days after PDT) the quantity of cells rapidly increased and exceeded the pre-irradiation value.

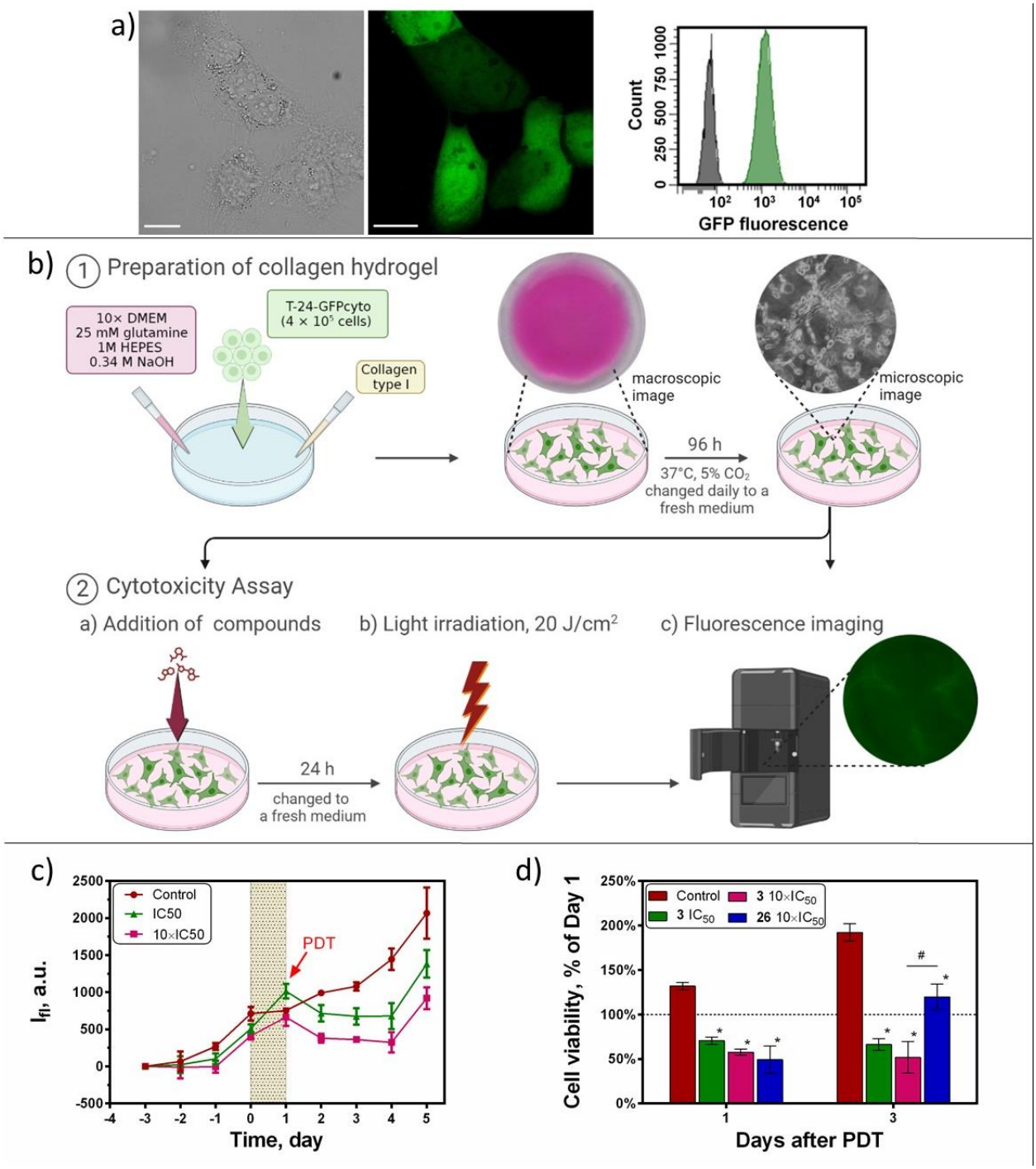

Figure 7. Anticancer activity of **3** in 3D *in vitro* model of tumor growth. a) Confocal images of T-24-GFP-cyto and plot of cell distribution by fluorescence signal level in a monoclonal cell line (T-24, grey) and TagGFP2-expressing cytoplasmic protein (T-24-GFP-cyto, green); b) Scheme of the experiment; c) Dynamics of changes in the fluorescence signal from hydrogels treated with **3** at concentrations IC_{50}(green) and 10 x IC_{50}(pink). The incubation time of **3** is indicated by a color mark. Photodynamic irradiation at dose 20 J/cm^2 was performed after 24 h incubation with **3** (marked by an arrow). d) Relative cell viability of T-24-GFP-cyto in 3D matrix on 1st day

and 3^{d} day after PDT using the conjugate **3** or the reference chlorin **26**. * - statistically significant difference from Control (Ordinary one-way ANOVA, Tukey's multiple comparisons test, $p < 0.05$). # - statistically significant difference from **26** (Ordinary one-way ANOVA, Tukey's multiple comparisons test, $p < 0.05$).

When comparing the results obtained for PDT alone (compound **26**) and the combination of photodynamic and targeted treatments (compound **3**), the most valuable effect of the suggested conjugation strategy is the substantial prolongation of the therapeutic effect. We attribute this phenomenon to the cytostatic behavior of cabozantinib, resulting in the death of cells-survivors after PDT. It is well established that sub-lethal PDT exposure can trigger cellular defense mechanisms and even promote cell growth [80, 81]. This undesired side effect can be mitigated by using pharmacological co-interventions. It is highly likely that the post-PDT continued effect of the cabozantinib derivative **5**, liberated from the conjugate **3**, prevented the cell proliferation and aggravate the cell stress. We hypothesize that a repeated treatment procedure and the adjustment of its regimen can drastically increase the lethality for the cancer cells and thus enhance the treatment efficiency.

4. Discussion and conclusions

Bladder cancer is known as a complex disease with high mortality and morbidity rates and refers to urothelial carcinoma of the proximal urethra and the upper urinary tract [82]. Depending on its stage, and localization, bladder cancers are categorized into non-muscle invasive bladder cancer (NMIBC) and muscle invasive bladder cancer (MIBC). Conventional techniques to treat NIMBC type of bladder cancer include a removal of the tumor with transurethral resection of bladder tumor (TURBT) followed by either intravesical Bacillus Calmette-Guerin (BCG) immunotherapy or chemotherapy. Even though these treatment protocols offer an immediate control over the tumor's progression, the nonspecific toxicity and a frequent recurrence represent major challenges to the treatment of NMIBC.

The first clinically approved PDT dates back to 1993 and involves the utilization of Photofrin® for the treatment of bladder cancer. Since then, only a limited number of PSs, namely, ALA derivatives (aminolaevulinic acid), have successfully entered the clinic for the NIMBC [47]. Although PDT demonstrated encouraging therapeutic results, further development has been largely obstructed due to a broad panel of adverse effects, mainly non-selective accumulation of PSs in normal urothelium [46, 47]. Recently, PDT of NIMBC has regained its popularity owing to advancement in tumor-targeting vectors and delivery vehicles. To date, a number of strategies have been successfully applied to improve selectivity during the NIMBC treatment [47]. Among them, the prodrug-based combination therapy, nanoparticles equipped with tumor-specific moieties, glycoconjugates and ADC (antibody-drug conjugates) hold a great promise.

In this study, we report the synthesis and the preliminary biological testing of multifunctional conjugate **3** addressing current challenges of PDT in the NIMBC treatment (Figure 8). To improve selectivity, we exploited the β-glucuronidase responsive linkage connected photosensitizing chlorin-e_6 (PDT module) and the cabozantinib derivative (TKI module). Such connection can be cleaved in the presence of β-glucuronidase, whose concentration is usually elevated in tumors [39] and in the urine of patients suffering from NIMBC [83]. Secondly, the selected TKI, the cabozantinib derivative **5**, served as a low-molecular weight ligand to tyrosine kinases, in particular, c-Met expressed in bladder cancers. The utilization of similar-type ligands, binding to corresponding tyrosine kinases, is a well-known paradigm in PDT to improve both selectivity [84] and enable combinational treatment [29]. Herein, we indeed observed that the cellular uptake of conjugate **3** was higher than that of reference chlorin-e_6 **26** lacking the cabozantinib unit. It was shown, that the primary cellular target of **3** are lysosomes, which is beneficial for PDT and can provide a media enriched with β-glucuronidase required for its successful activation. Interestingly, photophysical parameters of conjugate **3**, namely fluorescence and SO quantum yield, were greatly reduced before the cleavage.

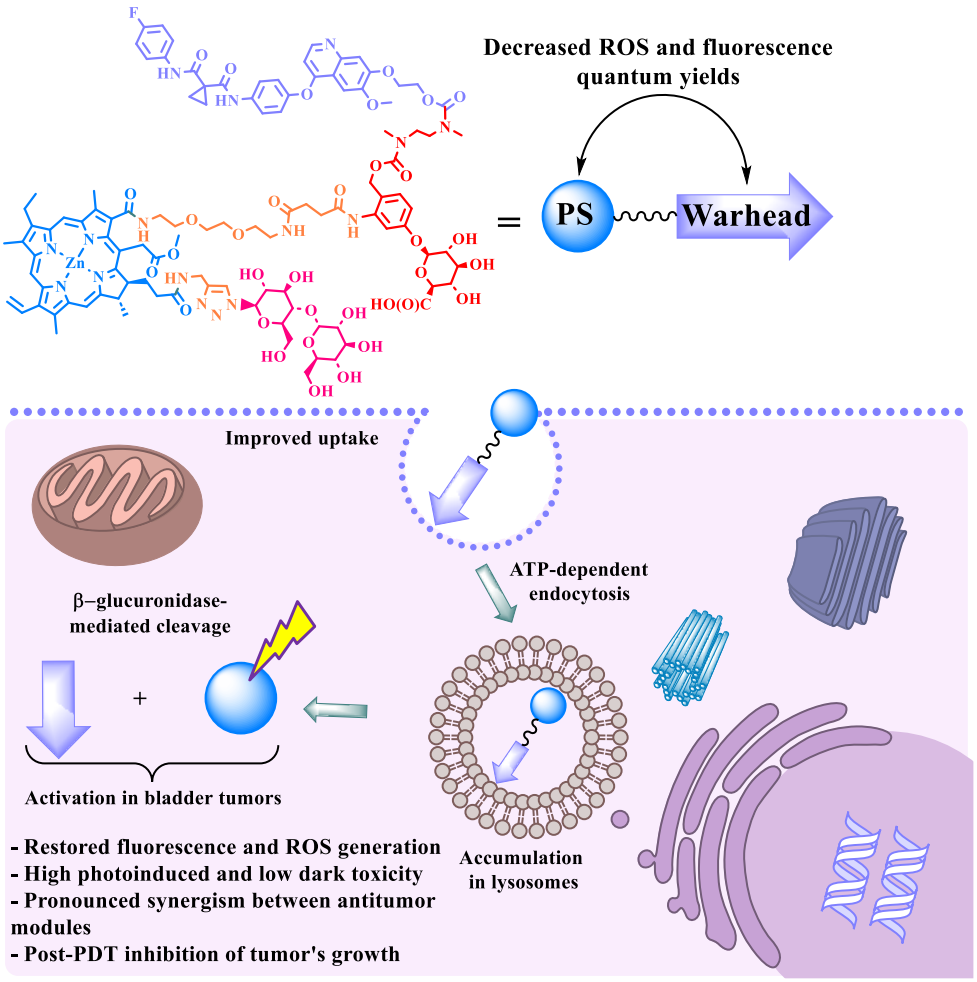

Figure 8. Summarized mode of action of multifunctional conjugate **3**.

Investigating the photodynamic activity of **3** in monolayer cell cultures and 3D *in vitro* tumor model, we also proved that conjugate **3** is a well-balanced photosensitizer with the unique ability to provide post-PDT therapeutic effects most likely due to the liberation of **5**. Altogether, the conjugate **3** offers three codependent levels of selectivity arising from its β-glucuronidase-mediated cleavage and the tyrosine kinase targeting.

Since the findings, presented in this study, are preliminary, we intent to conduct in-depth investigation of the post-PDT effect and its relevant biological targets. It is crucial to demonstrate that conjugate **3** can overcome recurrence of NIMBC by maintaining the sustainable inhibition of tumor's growth in dark. Apart from this, we also aim to further disclose the reasons behind improved accumulation of **3** in cells. It is essential to determine if the increased uptake is a result of cabozantinib's known inhibition of efflux pumps or its targeting of tyrosine kinases. Other important considerations are dwelling time and diffusion of **3**, which should be suitable for

intravesical injection. To study this, we plan to use appropriate spheroid and organoid models. Lastly, we are interested in elaboration on diagnostic potential of conjugate **3**, since its fluorescent response in principle can be indicative for the presence of β-glucuronidase-expressing tumors.

In conclusion, we developed the β-glucuronidase-responsive conjugate **3** based on the chlorin-e_6 photosensitizer and the cabozantinib derivative. While further elucidation is needed, the data obtained so far demonstrate that this conjugate offers a promising and comprehensive approach for the treatment of bladder cancers.

Author contributions

V.F.O., I.V.B., A.Yu.F. Conceptualization, Supervision and Project administration. A.V.N., H.-G.S. Funding acquisition and Project administration. V.F.O., L.V.K Investigation, Methodology, Visualization and Validation. V.F.O., L.V.K. Writing – original draft. V.F.O., I.V.B., A.Yu.F. Writing - review & editing. Y.V.R., O.I.K., S.Z.V., N.N.P. Resources. N.S.K., E.A.F. Data curation.

Declaration of Competing Interest

The authors declare no conflict of interest.

Data availability

Data will be made available on request.

Acknowledgments

This work was supported by the Russian Science Foundation under Grant No. 21-73-10230; https://rscf.ru/en/project/21-73-10230/.

Appendix A. Supplementary data

Supplementary data to this article can be found online at

References

[1] U. Chilakamarthi, L. Giribabu, Photodynamic Therapy: Past, Present and Future, Chem. Rec. 17 (8) (2017) 775–802. https://doi.org/10.1002/TCR.201600121.

[2] D. van Straten, V. Mashayekhi, H. S. de Bruijn, S. Oliveira, D. J. Robinson, Oncologic Photodynamic Therapy: Basic Principles, Current Clinical Status and Future Directions, Cancers 9 (2) (2017) 19. https://doi.org/10.3390/cancers9020019.

[3] S. Kwiatkowski, B. Knap, D. Przystupski, J. Saczko, E. Kędzierska, K. Knap-Czop, J. Kotlińska, O. Michel, K. Kotowski, J. Kulbacka, Photodynamic Therapy – Mechanisms, Photosensitizers and Combinations, Biomed. Pharmacother. 106 (2018) 1098–1107. https://doi.org/10.1016/j.biopha.2018.07.049.

[4] O. I. Koifman, T. A. Ageeva, N. S. Kuzmina, V. F. Otvagin, A. V. Nyuchev, A. Y. Fedorov, D. V. Belykh, N. S. Lebedeva, E. S. Yurina, S. A. Syrbu, M. O. Koifman, Y. A. Gubarev, D. A. Bunin, Y. G. Gorbunova, A. G. Martynov, A. Y. Tsivadze, S. V. Dudkin, A. V. Lyubimtsev, L. A. Maiorova, M. V. Kishalova, M. V. Petrova, V. B. Sheinin, V. S. Tyurin, I. A. Zamilatskov, E. I. Zenkevich, P. K. Morshnev, D. B. Berezin, E. A. Drondel, A. V. Kustov, V. A. Pogorilyy, A. N. Noev, E. A. Eshtukova-Shcheglova, E. A. Plotnikova, A. D. Plyutinskaya, N. B. Morozova, A. A. Pankratov, M. A. Grin, O. B. Abramova, E. A. Kozlovtseva, V. V. Drozhzhina, E. V. Filonenko, A. D. Kaprin, A. V. Ryabova, D. V. Pominova, I. D. Romanishkin, V. I. Makarov, V. B. Loschenov, K. A. Zhdanova, A. V. Ivantsova, Y. S. Bortnevskaya, N. A. Bragina, A. B. Solovieva, A. S. Kuryanova, P. S. Timashev, Synthesis Strategy of Tetrapyrrolic Photosensitizers for Their Practical Application in Photodynamic Therapy, Macroheterocycles 15 (4) (2022) 207–302. https://doi.org/10.6060/mhc224870k.

[5] D. Kessel, Apoptosis, Paraptosis and Autophagy: Death and Survival Pathways Associated with Photodynamic Therapy, Photochem. Photobiol. 95 (1) (2019) 119–125. https://doi.org/10.1111/PHP.12952.

[6] T. Mishchenko, I. Balalaeva, A. Gorokhova, M. Vedunova, D. V. Krysko, Which Cell Death Modality Wins the Contest for Photodynamic Therapy of Cancer? Cell Death Dis. 13 (5) (2022) 455. https://doi.org/10.1038/s41419-022-04851-4.

[7] Q. Chen, K. T. Li, S. Tian, T. H. Yu, L. H. Yu, H. D. Lin, D. Q. Bai, Photodynamic Therapy Mediated by Aloe-Emodin Inhibited Angiogenesis and Cell Metastasis Through Activating MAPK Signaling Pathway on HUVECs, Technol. Cancer Res. Treat. 17 (2018). https://doi.org/10.1177/1533033818785512.

[8] R. Alzeibak, T. A. Mishchenko, N. Y. Shilyagina, I. V. Balalaeva, M. V. Vedunova, D. V. Krysko, Targeting Immunogenic Cancer Cell Death by Photodynamic Therapy: Past, Present and Future. Journal for ImmunoTherapy of Cancer 9 (1) (2021) e001926. https://doi.org/10.1136/JITC-2020-001926.

[9] G. M. Cramer, E. K. Moon, K. A. Cengel, T. M. Busch, Photodynamic Therapy and Immune Checkpoint Blockade†, Photochem. Photobiol. 96 (5) (2020) 954–961. https://doi.org/10.1111/PHP.13300.

[10] I. S. Mfouo-Tynga, L. D. Dias, N. M. Inada, C. Kurachi, Features of Third Generation Photosensitizers Used in Anticancer Photodynamic Therapy: Review, Photodiagnosis Photodyn. Ther. 34 (2021) 102091. https://doi.org/10.1016/J.PDPDT.2020.102091.

[11] X. Deng, Z. Shao, Y. Zhao, Solutions to the Drawbacks of Photothermal and Photodynamic Cancer Therapy, Adv. Sci. 8 (3) (2021) 2002504. https://doi.org/10.1002/ADVS.202002504.

[12] X. Li, M. Gao, K. Xin, L. Zhang, D. Ding, D. Kong, Z. Wang, Y. Shi, F. Kiessling, T. Lammers, J. Cheng, Y. Zhao, Singlet Oxygen-Responsive Micelles for Enhanced Photodynamic Therapy, J. Control. Release 260 (2017) 12–21. https://doi.org/10.1016/J.JCONREL.2017.05.025.

[13] X. Li, N. Kwon, T. Guo, Z. Liu, J. Yoon, Innovative Strategies for Hypoxic-Tumor Photodynamic Therapy, Angew. Chemie Int. Ed. 57 (36) (2018) 11522–11531. https://doi.org/10.1002/ANIE.201805138.

[14] K. Komolibus, C. Fisher, J. Swartling, S. Svanberg, K. Svanberg, S. Andersson-Engels, Perspectives on Interstitial Photodynamic Therapy for Malignant Tumors, J. Biomed. Opt. 26 (7) (2021) 070604. https://doi.org/10.1117/1.JBO.26.7.070604.

[15] S. R. G. Fernandes, R. Fernandes, B. Sarmento, P. M. R. Pereira, J. P. C. Tomé, Photoimmunoconjugates: Novel Synthetic Strategies to Target and Treat Cancer by Photodynamic Therapy, Org. Biomol. Chem. 17 (10) (2019) 2579–2593. https://doi.org/10.1039/C8OB02902D.

[16] J. C. H. Chu, W. P. Fong, C. T. T. Wong, D. K. P. Ng, Facile Synthesis of Cyclic Peptide-Phthalocyanine Conjugates for Epidermal Growth Factor Receptor-Targeted Photodynamic Therapy, J. Med. Chem. 64 (4) (2021) 2064–2076. https://doi.org/10.1021/acs.jmedchem.0c01677.
[17] G. Durán-Sampedro, E. Y. Xue, M. Moreno-Simoni, C. Paramio, T. Torres, D. K. P. Ng, G. de la Torre, Glycosylated BODIPY- Incorporated Pt(II) Metallacycles for Targeted and Synergistic Chemo-Photodynamic Therapy, J. Med. Chem. 66 (5) (2023) 3448–3459. https://doi.org/10.1021/acs.jmedchem.2c01940.
[18] R. R. Cheruku, J. Cacaccio, F. A. Durrani, W. A. Tabaczynski, R. Watson, A. Marko, R. Kumar, M. E. El-Khouly, S. Fukuzumi, J. R. Missert, R. Yao, M. Sajjad, D. Chandra, K. Guru, R. K. Pandey, Epidermal Growth Factor Receptor-Targeted Multifunctional Photosensitizers for Bladder Cancer Imaging and Photodynamic Therapy, J. Med. Chem. 62 (5) (2019) 2598–2617. https://doi.org/10.1021/acs.jmedchem.8b01927.
[19] F. L. Zhang, Q. Huang, J. Y. Liu, M. D. Huang, J. P. Xue, Molecular-Target-Based Anticancer Photosensitizer: Synthesis and in Vitro Photodynamic Activity of Erlotinib-Zinc(II) Phthalocyanine Conjugates, ChemMedChem 10 (2) (2015) 312–320. https://doi.org/10.1002/cmdc.201402373.
[20] R. R. Cheruku, J. Cacaccio, F. A. Durrani, W. A. Tabaczynski, R. Watson, K. Siters, J. R. Missert, E. C. Tracy, M. Dukh, K. Guru, R. C. Koya, P. Kalinski, H. Baumann, R. K. Pandey, Synthesis, Tumor Specificity, and Photosensitizing Efficacy of Erlotinib-Conjugated Chlorins and Bacteriochlorins: Identification of a Highly Effective Candidate for Photodynamic Therapy of Cancer, J. Med. Chem. 64 (1) (2021) 741–767. https://doi.org/10.1021/acs.jmedchem.0c01735.
[21] G. Wei, L. Huang, Y. Jiang, Y. Shen, Z. Huang, Y. Huang, X. Sun, C. Zhao, Lenvatinib-Zinc Phthalocyanine Conjugates as Potential Agents for Enhancing Synergistic Therapy of Multidrug-Resistant Cancer by Glutathione Depletion, Eur. J. Med. Chem. 169 (2019) 53–64. https://doi.org/10.1016/j.ejmech.2019.02.065.
[22] Y. S. Bortnevskaya, N. A. Shiryaev, N. S. Zakharov, O. O. Kitoroage, M. A. Gradova, N. Y. Karpechenko, A. S. Novikov, E. D. Nikolskaya, M. R. Mollaeva, N. G. Yabbarov, N. A. Bragina, K. A. Zhdanova, Synthesis and Biological Properties of EGFR-Targeted Photosensitizer Based on Cationic Porphyrin, Pharm. 15 (4) (2023) 1284. https://doi.org/10.3390/pharmaceutics15041284.
[23] N. S. Kuzmina, V. F. Otvagin, A. A. Maleev, M. A. Urazaeva, A. V. Nyuchev, S. K. Ignatov, A. E. Gavryushin, A. Y. Fedorov, Development of Novel Porphyrin/Combretastatin A-4 Conjugates for Bimodal Chemo and Photodynamic Therapy: Synthesis, Photophysical and TDDFT Computational Studies, J. Photochem. Photobiol. A Chem. 433 (2022) 114138. https://doi.org/10.1016/j.jphotochem.2022.114138.
[24] E. Ortega-Forte, A. Rovira, A. Gandioso, J. Bonelli, M. Bosch, J. Ruiz, V. Marchán, COUPY Coumarins as Novel Mitochondria-Targeted Photodynamic Therapy Anticancer Agents, J. Med. Chem. 64 (23) (2021) 17209–17220. https://doi.org/10.1021/acs.jmedchem.1c01254.
[25] R. Wang, X. Li, J. Yoon, Organelle-Targeted Photosensitizers for Precision Photodynamic Therapy, ACS Appl. Mater. Interfaces 13 (17) (2021) 19543–19571. https://doi.org/10.1021/acsami.1c02019.
[26] Y. Liu, Q. Li, M. Gu, D. Lu, X. Xiong, Z. Zhang, Y. Pan, Y. Liao, Q. Ding, W. Gong, D. S. Chen, M. Guan, J. Wu, Z. Tian, H. Deng, L. Gu, X. Hong, Y. Xiao, A Second Near-Infrared Ru(II) Polypyridyl Complex for Synergistic Chemo-Photothermal Therapy, J. Med. Chem. 65 (3) (2022) 2225–2237. https://doi.org/10.1021/acs.jmedchem.1c01736.
[27] C. J. Zhang; Q. Hu; G. Feng; R. Zhang; Y. Yuan; X. Lu; B. Liu, Image-Guided Combination Chemotherapy and Photodynamic Therapy Using a Mitochondria-Targeted Molecular Probe with Aggregation-Induced Emission Characteristics, Chem. Sci. 6 (8) (2015) 4580–4586. https://doi.org/10.1039/C5SC00826C.
[28] G. D. Wang, H. T. Nguyen, H. Chen, P. B. Cox, L. Wang, K. Nagata, Z. Hao, A. Wang, Z. Li, J. Xie, X-Ray Induced Photodynamic Therapy: A Combination of Radiotherapy and Photodynamic Therapy, Theranostics 6 (13) (2016) 2295–2305. https://doi.org/10.7150/thno.16141.
[29] V. F. Otvagin, N. S. Kuzmina, E. S. Kudriashova, A. V. Nyuchev, A. E. Gavryushin, A. Y. Fedorov, Conjugates of Porphyrinoid-Based Photosensitizers with Cytotoxic Drugs: Current Progress and Future Directions toward Selective Photodynamic Therapy, J. Med. Chem. 65 (3) (2022) 1695–1734. https://doi.org/10.1021/acs.jmedchem.1c01953.
[30] M. Grin, N. Suvorov, P. Ostroverkhov, V. Pogorilyy, N. Kirin, A. Popov, A. Sazonova, E. Filonenko, Advantages of Combined Photodynamic Therapy in the Treatment of Oncological Diseases, Biophys. Rev. 14 (4) (2022) 941–963. https://doi.org/10.1007/s12551-022-00962-6.
[31] V. F. Otvagin, A. V. Nyuchev, N. S. Kuzmina, I. D. Grishin, A. E. Gavryushin, Y. V. Romanenko, O. I.

Koifman, D. V. Belykh, N. N. Peskova, N. Y. Shilyagina, I. V. Balalaeva, A. Y. Fedorov, Synthesis and Biological Evaluation of New Water-Soluble Photoactive Chlorin Conjugate for Targeted Delivery, Eur. J. Med. Chem. 144 (2018) 740–750. https://doi.org/10.1016/j.ejmech.2017.12.062.

[32] V. F. Otvagin, N. S. Kuzmina, L. V. Krylova, A. B. Volovetsky, A. V. Nyuchev, A. E. Gavryushin, I. N. Meshkov, Y. G. Gorbunova, Y. V. Romanenko, O. I. Koifman, I. V Balalaeva, A. Y. Fedorov, Water-Soluble Chlorin/Arylaminoquinazoline Conjugate for Photodynamic and Targeted Therapy, J. Med. Chem. 62 (24) (2019) 11182–11193. https://doi.org/10.1021/acs.jmedchem.9b01294.

[33] A. V. Nyuchev, V. F. Otvagin, A. E. Gavryushin, Y. I. Romanenko, O. I. Koifman, D. V. Belykh, H. G. Schmalz, A. Y. Fedorov, Synthesis of Chlorin–(Arylamino)Quinazoline Hybrids as Models for Multifunctional Drug Development, Synthesis 47 (23) (2015) 3717–3726. https://doi.org/10.1055/S-0034-1378876.

[34] A. Abdelaziz, U. Vaishampayan, Cabozantinib for the Treatment of Kidney Cancer, Expert Rev. Anticancer Ther. 17 (7) (2017) 577–584. https://doi.org/10.1080/14737140.2017.1344553.

[35] F. M. Yakes, J. Chen, J. Tan, K. Yamaguchi, Y. Shi, P. Yu, F. Qian, F. Chu, F. Bentzien, B. Cancilla, J. Orf, A. You, A. D. Laird, S. Engst, L. Lee, J. Lesch, Y. C. Chou, A. H. Joly, Cabozantinib (XL184), a Novel MET and VEGFR2 Inhibitor, Simultaneously Suppresses Metastasis, Angiogenesis, and Tumor Growth, Mol. Cancer Ther. 10 (12) (2011) 2298–2308. https://doi.org/10.1158/1535-7163.MCT-11-0264.

[36] L. Marandino, D. Raggi, G. Calareso, A. Alessi, M. Colecchia, A. Martini, A. Briganti, F. Montorsi, R. Madison, J. S. Ross, A. Necchi, Cabozantinib Plus Durvalumab in Patients With Advanced Urothelial Carcinoma After Platinum Chemotherapy: Safety and Preliminary Activity of the Open-Label, Single-Arm, Phase 2 ARCADIA Trial, Clin. Genitourin. Cancer 19 (5) (2021) 457–465. https://doi.org/10.1016/j.clgc.2021.04.001.

[37] A. B. Apolo, R. Nadal, Y. Tomita, N. N. Davarpanah, L. M. Cordes, S. M. Steinberg, L. Cao, H. L. Parnes, R. Costello, M. J. Merino, L. R. Folio, L. Lindenberg, M. Raffeld, J. Lin, M. J. Lee, S. Lee, S. V. Alarcon, A. Yuno, N. A. Dawson, K. Allette, A. Roy, D. De Silva, M. M. Lee, T. M. Sissung, W. D. Figg, P. K. Agarwal, J. J. Wright, Y. M. Ning, J. L. Gulley, W. L. Dahut, D. P. Bottaro, J. B. Trepel, Cabozantinib in Patients with Platinum-Refractory Metastatic Urothelial Carcinoma: An Open-Label, Single-Centre, Phase 2 Trial, Lancet Oncol. 21 (8) (2020) 1099–1109. https://doi.org/10.1016/S1470-2045(20)30202-3.

[38] J. N. Markowitz, K. M. Fancher, Cabozantinib: A Multitargeted Oral Tyrosine Kinase Inhibitor, Pharmacother. J. Hum Pharmacol. Drug Ther. 38 (3) (2018) 357–369. https://doi.org/10.1002/PHAR.2076.

[39] I. Tranoy-Opalinski, T. Legigan, R. Barat, J. Clarhaut, M. Thomas, B. Renoux, S. Papot, β-Glucuronidase-Responsive Prodrugs for Selective Cancer Chemotherapy: An Update, Eur. J. Med. Chem. 74 (2014) 302–313. https://doi.org/10.1016/j.ejmech.2013.12.045.

[40] P. Awolade, N. Cele, N. Kerru, L. Gummidi, E. Oluwakemi, P. Singh, Therapeutic Significance of β-Glucuronidase Activity and Its Inhibitors: A Review, Eur. J. Med. Chem. 187 (2020) 111921. https://doi.org/10.1016/j.ejmech.2019.111921.

[41] S. C. Jeffrey, J. B. Andreyka, S. X. Bernhardt, K. M. Kissler, T. Kline, J. S. Lenox, R. F. Moser, M. T. Nguyen, N. M. Okeley, I. J. Stone, X. Zhang, P. D. Senter, Development and Properties of β-Glucuronide Linkers for Monoclonal Antibody-Drug Conjugates, Bioconjug. Chem. 17 (3) (2006) 831–840. https://doi.org/10.1021/bc0600214.

[42] S. C. Jeffrey, J. De Brabander, J. Miyamoto, P. D. Senter, Expanded Utility of the β-Glucuronide Linker: ADCs That Deliver Phenolic Cytotoxic Agents, ACS Med. Chem. Lett. 1 (6) (2010) 277–280. https://doi.org/10.1021/ml100039h.

[43] S. Singh, A. Aggarwal, N. V. S. D. K. Bhupathiraju, G. Arianna, K. Tiwari, C. M. Drain, Glycosylated Porphyrins, Phthalocyanines, and Other Porphyrinoids for Diagnostics and Therapeutics, Chem. Rev. 115 (18) (2015) 10261–10306. https://doi.org/10.1021/acs.chemrev.5b00244.

[44] N. S. Kuzmina, V. F. Otvagin, L. V. Krylova, A. V. Nyuchev, Y. V. Romanenko, O. I. Koifman, I. V. Balalaeva, A. Y. Fedorov, Synthesis and Antiproliferative Activity of New Chlorin E6 Glycoconjugates, Mendeleev Commun. 30 (2) (2020) 159–161. https://doi.org/10.1016/j.mencom.2020.03.009.

[45] C. C. Barron, P. J. Bilan, T. Tsakiridis, E. Tsiani, Facilitative Glucose Transporters: Implications for Cancer Detection, Prognosis and Treatment, Metabolism 65 (2) (2016) 124–139. https://doi.org/10.1016/j.metabol.2015.10.007.

[46] R. Railkar, P. K. Agarwal, Photodynamic Therapy in the Treatment of Bladder Cancer: Past Challenges

and Current Innovations, Eur. Urol. Focus 4 (4) (2018) 509–511. https://doi.org/10.1016/j.euf.2018.08.005.
[47] K. M. M. Rahman, P. Giram, B. A. Foster, Y. You, Photodynamic Therapy for Bladder Cancers, A Focused Review†, Photochem. Photobiol. 99 (2) (2023) 420–436. https://doi.org/10.1111/php.13726.
[48] K. M. M. Rahman, P. Thapa, R. Hurst, S. Woo, Y. You, Singlet Oxygen Activatable Prodrugs of Paclitaxel, SN-38, MMC and CA4: Nonmitochondria-Targeted Prodrugs†, Photochem. Photobiol. 98 (2) (2022) 389–399. https://doi.org/10.1111/php.13589.
[49] M. Bio, P. Rajaputra, I. Lim, P. Thapa, B. Tienabeso, R. E. Hurst, Y. You, Efficient Activation of a Visible Light-Activatable CA4 Prodrug through Intermolecular Photo-Unclick Chemistry in Mitochondria, Chem. Commun. 53 (11) (2017) 1884–1887. https://doi.org/10.1039/C6CC09994G.
[50] L. Bourré, G. Simonneaux, Y. Ferrand, S. Thibaut, Y. Lajat, T. Patrice, Synthesis, and in Vitro and in Vivo Evaluation of a Diphenylchlorin Sensitizer for Photodynamic Therapy, J. Photochem. Photobiol. B Biol. 69 (3) (2003) 179–192. https://doi.org/10.1016/S1011-1344(03)00020-4.
[51] N. Y. Shilyagina, V. I. Plekhanov, I. V. Shkunov, P. A. Shilyagin, L. V. Dubasova, A. A. Brilkina, E. A. Sokolova, I. V. Turchin, I. V. Balalaeva, LED Light Source for In Vitro Study of Photosensitizing Agents for Photodynamic Therapy, Sovrem. Tehnol. Med. 8 (2014) 15−24.
[52] I. E. Kochevar, C. R. Lambert, M. C. Lynch, A. C. Tedesco, Comparison of Photosensitized Plasma Membrane Damage Caused by Singlet Oxygen and Free Radicals, Biochim. Biophys. Acta - Biomembr. 1280 (2) (1996) 223–230. https://doi.org/10.1016/0005-2736(95)00297-9.
[53] T. Mosmann, Rapid Colorimetric Assay for Cellular Growth and Survival: Application to Proliferation and Cytotoxicity Assays, J. Immunol. Methods 65 (1–2) (1983) 55–63. https://doi.org/10.1016/0022-1759(83)90303-4.
[54] L. M. Sencha, A. A. Gorokhova, N. N. Peskova, E. I. Cherkasova, I. V. Balalaeva, Dynamic Study of PDT-Induced Oxidative Stress in Cancer Cells Embedded in 3D Collagen Hydrogel Using Genetically Encoded H2O2-Sensor, J. Biomed. Photonics Eng. 8 (4) (2022) 040305. https://doi.org/10.18287/JBPE22.08.040305.
[55] L. C. Bannen, D. S.-M. Chan, J. Chen, L. E. Dalrymple, T. P. Forsyth, T. P. Huynh, V. Jammalamadaka, R. G. Khoury, J. W. Leahy, M. B. Mac, G. Mann, L. W. Mann, J. M. Nuss, J. J. Parks, C. S. Takeuchi, Y. Wang, W. Xu, C-Met Modulators And Methods Of Use, WO2005030140A2, 2012.
[56] Z. Vazifehasl, S. Hemmati, M. Zamanloo, M. Jaymand, Synthesis and Characterization of Novel Diglycidyl Methacrylate-Based Macromonomers on Isosorbide for Dental Composites, Macromol. Res. 21 (2013) 427–434. https://doi.org/10.1007/S13233-013-1038-1.
[57] F. Aguilar, U.R. Charrondiere, B. Dusemund, P. Galtier, J. Gilbert, D.M. Gott, S. Grilli, R. Guertler, G.E.N. Kass, J. Koenig, C. Lambré, J-C. Larsen, J-C. Leblanc, A. Mortensen, D. Parent-Massin, I. Pratt, I.M.C.M. Rietjens, I. Stankovic, P. Tobback, T. Verguieva, R.A. Woutersen, The Use of Taurine and D-Glucurono-γ-Lactone as Constituents of the so-Called “Energy” Drinks, EFSA J. 935 (2009) 1–31. https://doi.org/10.2903/J.EFSA.2009.935.
[58] T. C. Cheng, S. R. Roffler, S. C. Tzou, K. H. Chuang, Y. C. Su, C. H. Chuang, C. H. Kao, C. S. Chen, I. H. Harn, K. Y. Liu, T. L. Cheng, Y. L. Leu, An Activity-Based near-Infrared Glucuronide Trapping Probe for Imaging β-Glucuronidase Expression in Deep Tissues, J. Am. Chem. Soc. 134 (6) (2012) 3103–3110. https://doi.org/10.1021/ja209335z.
[59] A. A. D’souza, R. Shegokar, Polyethylene Glycol (PEG): A Versatile Polymer for Pharmaceutical Applications, Expert Opin. Drug Deliv. 13 (9) (2016) 1257–1275. https://doi.org/10.1080/17425247.2016.1182485.
[60] J. M. Dąbrowski, L. G. Arnaut, M. M. Pereira, K. Urbańska, S. Simões, G. Stochel, L. Cortes, Combined Effects of Singlet Oxygen and Hydroxyl Radical in Photodynamic Therapy with Photostable Bacteriochlorins: Evidence from Intracellular Fluorescence and Increased Photodynamic Efficacy in Vitro, Free Radic. Biol. Med. 52 (7) (2012) 1188–1200. https://doi.org/10.1016/j.freeradbiomed.2011.12.027.
[61] C. W. Lindsley, Lipophilicity, in: I. P. Stolerman, L. H. Price (Eds.), Encyclopedia of Psychopharmacology, Springer, Berlin, Heidelberg, 2010, pp. 1–6.
[62] M. R. Ke, S. F. Chen, X. H. Peng, Q. F. Zheng, B. Y. Zheng, C. K. Yeh, J. D. Huang, A Tumor-Targeted Activatable Phthalocyanine-Tetrapeptide-Doxorubicin Conjugate for Synergistic Chemo-Photodynamic Therapy, Eur. J. Med. Chem. 127 (2017) 200–209. https://doi.org/10.1016/j.ejmech.2016.12.056.
[63] Z. Hu, Y. Lin, H. Chen, Y. Mao, J. Wu, Y. Zhu, X. Xu, X. Xu, S. Li, X. Zheng, L. Xie, MicroRNA-101 Suppresses Motility of Bladder Cancer Cells by Targeting c-Met, Biochem. Biophys. Res. Commun.

435 (1) (2013) 82–87. https://doi.org/10.1016/J.BBRC.2013.04.042.
[64] G. N. Zhang, Y. K. Zhang, Y. J. Wang, A. M. Barbuti, X. J. Zhu, X. Y. Yu, A. W. Wen, J. N. D. Wurpel, Z. S. Chen, Modulating the Function of ATP-Binding Cassette Subfamily G Member 2 (ABCG2) with Inhibitor Cabozantinib, Pharmacol. Res. 119 (2017) 89–98. https://doi.org/10.1016/J.PHRS.2017.01.024.
[65] R. W. Robey, K. Steadman, O. Polgar, S. E. Bates, ABCG2-Mediated Transport of Photosensitizers: Potential Impact on Photodynamic Therapy, Cancer Biol. Ther. 4 (2) (2005) 195–202. https://doi.org/10.4161/cbt.4.2.1440.
[66] L. Qiao, J. Liu, Y. Han, F. Wei, X. Liao, C. Zhang, L. Xie, L. Ji, H. Chao, Rational Design of a Lysosome-Targeting and near-Infrared Absorbing Ru(II)–BODIPY Conjugate for Photodynamic Therapy, Chem. Commun. 57 (14) (2021) 1790–1793. https://doi.org/10.1039/D0CC06926D.
[67] C. Figliola, H. Anton, C. Sutter, C. Chériaux, A. Sutter, V. Mazan, M. Elhabiri, P. Didier, D. Jacquemin, G. Ulrich, Lysosomes Targeting PH Activable Imaging-Guided Photodynamic Agents. ChemBioChem 24 (12) (2023) e202300139. https://doi.org/10.1002/CBIC.202300139.
[68] D. Kessel, N. L. Oleinick, Cell Death Pathways Associated with Photodynamic Therapy: An Update, Photochem. Photobiol. 94 (2) (2018) 213–218. https://doi.org/10.1111/php.12857.
[69] T. Shintani, Y. Kusuhara, K. Daizumoto, T. O. Dondoo, H. Yamamoto, H. Mori, T. Fukawa, H. Nakatsuji, T. Fukumori, M. Takahashi, H. Kanayama, The Involvement of Hepatocyte Growth Factor-MET-Matrix Metalloproteinase 1 Signaling in Bladder Cancer Invasiveness and Proliferation. Effect of the MET Inhibitor, Cabozantinib (XL184), on Bladder Cancer Cells, Urology 101 (2017) 169.e7-169.e13. https://doi.org/10.1016/j.urology.2016.12.006.
[70] L. Zhao, M. G. Wientjes, J. L. S. Au, Evaluation of Combination Chemotherapy: Integration of Nonlinear Regression, Curve Shift, Isobologram, and Combination Index Analyses, Clin. Cancer Res. 10 (23) (2004) 7994–8004. https://doi.org/10.1158/1078-0432.CCR-04-1087.
[71] K. A. Fitzgerald, M. Malhotra, C. M. Curtin, F. J. O' Brien, C. M. O' Driscoll, Life in 3D Is Never Flat: 3D Models to Optimise Drug Delivery, J. Control. Release 215 (2015) 39–54. https://doi.org/10.1016/j.jconrel.2015.07.020.
[72] F. Klemm, J. A. Joyce, Microenvironmental Regulation of Therapeutic Response in Cancer, Trends Cell Biol. 25 (4) (2015) 198–213. https://doi.org/10.1016/J.TCB.2014.11.006.
[73] O. M. Kutova, A. D. Pospelov, I. V. Balalaeva, The Multifaceted Role of Connexins in Tumor Microenvironment Initiation and Maintenance, Biol. 12 (2) (2023) 204. https://doi.org/10.3390/biology12020204.
[74] M. A. Harding, D. Theodorescu, RhoGDI2: A New Metastasis Suppressor Gene: Discovery and Clinical Translation, Urol. Oncol. Semin. Orig. Investig. 25 (5) (2007) 401–406. https://doi.org/10.1016/j.urolonc.2007.05.006.
[75] T. Naito, T. Higuchi, Y. Shimada, C. Kakinuma, An Improved Mouse Orthotopic Bladder Cancer Model Exhibiting Progression and Treatment Response Characteristics of Human Recurrent Bladder Cancer, Oncol. Lett. 19 (1) (2020) 833–839. https://doi.org/10.3892/OL.2019.11172.
[76] L. M. Sencha, O. E. Dobrynina, A. D. Pospelov, E. L. Guryev, N. N. Peskova, A. A. Brilkina, E. I. Cherkasova, I. V. Balalaeva, Real-Time Fluorescence Visualization and Quantitation of Cell Growth and Death in Response to Treatment in 3D Collagen-Based Tumor Model, Int. J. Mol. Sci. 23 (16) (2022) 8837. https://doi.org/10.3390/IJMS23168837.
[77] O. M. Kutova, L. M. Sencha, A. D. Pospelov, O. E. Dobrynina, A. A. Brilkina, E. I. Cherkasova, I. V. Balalaeva, Comparative Analysis of Cell–Cell Contact Abundance in Ovarian Carcinoma Cells Cultured in Two- and Three-Dimensional In Vitro Models, Biol. 9 (12) (2020) 446. https://doi.org/10.3390/biology9120446.
[78] E. A. Sokolova, V. A. Vodeneev, S. M. Deyev, I. V. Balalaeva, 3D in Vitro Models of Tumors Expressing EGFR Family Receptors: A Potent Tool for Studying Receptor Biology and Targeted Drug Development, Drug Discov. Today 24 (1) (2019) 99–111. https://doi.org/10.1016/j.drudis.2018.09.003.
[79] M. Kucinska, A. Plewinski, W. Szczolko, M. Kaczmarek, T. Goslinski, M. Murias, Modeling the Photodynamic Effect in 2D versus 3D Cell Culture under Normoxic and Hypoxic Conditions, Free Radic. Biol. Med. 162 (2021) 309–326. https://doi.org/10.1016/j.freeradbiomed.2020.10.304.
[80] R. Weijer, S. Clavier, E. A. Zaal, M. M. E. Pijls, R. T. van Kooten, K. Vermaas, R. Leen, A. Jongejan, P. D. Moerland, A. H. C. van Kampen, A. B. P. van Kuilenburg, C. R. Berkers, S. Lemeer, M. Heger, Multi-OMIC Profiling of Survival and Metabolic Signaling Networks in Cells Subjected to Photodynamic Therapy, Cell. Mol. Life Sci. 74 (6) (2017) 1133–1151. https://doi.org/10.1007/S00018-016-2401-0.

[81] M. Broekgaarden, R. Weijer, T. M. van Gulik, M. R. Hamblin, M. Heger, Tumor Cell Survival Pathways Activated by Photodynamic Therapy: A Molecular Basis for Pharmacological Inhibition Strategies, Cancer Metastasis Rev. 34 (4) (2015) 643–690. https://doi.org/10.1007/S10555-015-9588-7.
[82] A. M. Kamat, N. M. Hahn, J. A. Efstathiou, S. P. Lerner, P. U. Malmström, W. Choi, C. C. Guo, Y. Lotan, W. Kassouf, Bladder Cancer, Lancet 388 (10061) (2016) 2796–2810. https://doi.org/10.1016/S0140-6736(16)30512-8.
[83] W. G. Haije, B. H. P. van der Werf-Messing, Some Investigations into the Origin of the β-Glucuronidase Activity in the Urine of Patients with Cancer of the Bladder, Br. J. Cancer 16 (3) (1962) 570–576. https://doi.org/10.1038/BJC.1962.66.
[84] L. Ulfo, P. E. Costantini, M. Di Giosia, A. Danielli, M. Calvaresi, EGFR-Targeted Photodynamic Therapy, Pharm. 14 (2) (2022) 241. https://doi.org/10.3390/pharmaceutics14020241.